

Bislug Flow in Circular and Noncircular Channels and the Role of  
Interface Stretching on Energy Dissipation

By

Joseph E. Hernandez

A THESIS

Submitted in partial fulfillment of the requirements

for the degree of

Master of Science in Mechanical Engineering

MICHIGAN TECHNOLOGICAL UNIVERSITY

August, 2008

This thesis, "Bislug Flow in Circular and Noncircular Channels and the Role of Interface Stretching on Energy Dissipation" is hereby approved in partial fulfillment of the requirements of the Degree of Master of Science in Mechanical Engineering.

Department of Mechanical Engineering - Engineering Mechanics

Advisor: \_\_\_\_\_  
Dr. Jeffrey S. Allen

Committee Member: \_\_\_\_\_  
Dr. Dennis DeSheng Meng

Committee Member: \_\_\_\_\_  
Dr. Ryan J. Gilbert

Department Chair: \_\_\_\_\_  
Professor William W. Predebon

Date: \_\_\_\_\_

## ABSTRACT

The area of microfluidics has increased in popularity with such fields as MEMS, microreactors, microscale heat exchangers, etc. A comprehensive understanding of dissipation mechanisms for fluid flow in microchannels is required to accurately predict the behavior in these small systems. Tests were performed using a constant pressure potential created by two immiscible fluids juxtaposed in a microchannel. This study focused on the flow and dissipation mechanisms in round and square microchannels. There are four major dissipation mechanisms in slug flow; wall shear, dissipation at the contact line, menisci interaction and the stretching of the interface. A force balance between the internal driving potential, viscous drag and interface stretching was used to develop a model for the prediction of the velocity of a bislug in a microchannel. Interface stretching is a dissipation mechanism that has been included due to the unique system properties and becomes increasingly more important as the bislug decreases in length.

# CONTENTS

<i>Table of Contents</i> . . . . .	v
<i>List of Figures</i> . . . . .	vii
<i>List of Tables</i> . . . . .	viii
<i>1. Introduction</i> . . . . .	1
1.1 <i>bislug Definition</i> . . . . .	1
1.2 <i>Motivation</i> . . . . .	1
<i>2. Background</i> . . . . .	3
2.1 <i>Capillary Systems</i> . . . . .	3
2.2 <i>Spontaneous Flow</i> . . . . .	5
2.3 <i>Coating Flows</i> . . . . .	6
2.4 <i>Corners</i> . . . . .	8
<i>3. Experimental Setup</i> . . . . .	10
<i>4. Numerical Modeling</i> . . . . .	14
4.1 <i>Velocity Profiles</i> . . . . .	14
4.2 <i>Force Balance</i> . . . . .	19
<i>5. Results and Discussion</i> . . . . .	27
5.1 <i>Round Microchannels</i> . . . . .	27
5.2 <i>Square Microchannels</i> . . . . .	30
<i>6. Force Terms</i> . . . . .	37
6.1 <i>Hydrodynamic Interaction</i> . . . . .	37
6.2 <i>Contact Line</i> . . . . .	37
6.3 <i>Non-Poiseuille flow</i> . . . . .	38
6.4 <i>Corner Flow</i> . . . . .	39
<i>7. Conclusion</i> . . . . .	40
<i>Appendix</i> . . . . .	41
<i>A. Confocal Imaging of Corner Flow</i> . . . . .	42

A.1 Sandia . . . . .	42
<i>B. Round Derivation</i> . . . . .	44
B.1 Derivation of Force Terms . . . . .	44
<i>C. Square Derivation</i> . . . . .	50
C.1 Derivation of Force Terms . . . . .	50
C.2 Drag . . . . .	52
C.3 Force Balance . . . . .	56

## LIST OF FIGURES

1.1	Bislug in a round microchannel, the dyed liquid is ethylene glycol and the non-dyed fluid is silicone oil. . . . .	1
1.2	Schematic of a bislug. . . . .	1
1.3	Schematic of passive pump . . . . .	2
2.1	A wetting fluid rises in a capillary while a non-wetting fluid will recede	3
2.2	Configuration of a liquid drop on a solid surrounded by a gas, the intersection of the three materials create the contact line. . . . .	4
2.3	A wetting system has a contact angle $< 90^\circ$ , water on clean glass, and a non-wetting system has a contact angle $> 90^\circ$ , water on wax coated glass.ref . . . . .	5
2.4	Spontaneous flow induced in a microchannel from a pressure imbalanced caused by a (a) difference in surface tension, (b)change in channel dimensions, and/or (c) change in contact angle.?? . . . . .	6
2.5	Schematic of a bislug during flow, both fluids A and B leave a thin film behind. . . . .	7
2.6	Coating profiles of liquid films in different channel geometries. . . . .	8
2.7	Spontaneous wicking of a fluid into a corner satisfying the Concus-Finn Criteria. . . . .	8
2.8	The schematic of a wedge with spontaneous corner wicking. . . . .	9
3.1	Experimental setup. . . . .	11
3.2	Bislug test fixture. . . . .	11
4.1	Assumed flow profiles of the Core and film used in the derivation of the models. . . . .	15
4.2	Flow profiles for the dry channels. . . . .	16
4.3	zoomed flow profiles for the dry channels. . . . .	17
4.4	Flow profiles for the prewet channels. . . . .	18
4.5	zoomed flow profiles for the prewet channels. . . . .	19
4.6	Geometry for the square channels. The square profile has eight symmetric sections, each of the sections has the profile on the right . . . .	19
4.7	high- profiles without films . . . . .	20
4.8	high-profiles with film . . . . .	20
4.9	high-Prewet flow profiles lines . . . . .	20
4.10	high-film velocity . . . . .	20
4.11	High Ca Number profiles . . . . .	20
4.12	low-profiles witout films . . . . .	21

4.13	low-profiles with film . . . . .	21
4.14	low-Prewet flow profiles lines . . . . .	21
4.15	low-film velocities . . . . .	21
4.16	Low Ca Number profiles . . . . .	21
4.17	Drag forces in a round channel, because of the small change in surface area the drag forces overlap. . . . .	23
4.18	The drag in a square channel, the circle and square are the boundaries used for data comparison, low Ca and high Ca. . . . .	25
5.1	The prewet and non-prewet round data. . . . .	28
5.2	Ca numbers for both the model and the Prewet data, the model is based on equation ?? using a ratio of $L_B/L_A = .5, 1, 2$ . . . . .	29
5.3	Bislug in a square channel. . . . .	30
5.4	Fluid retention in the corner of a prewet square microchannel. . . . .	30
5.5	Graph of Ca for square dry channel . . . . .	31
5.6	Images used to estimated the film thickness on the walls of a square microchannel. (a) Used for scaling images. (b) and (c) Used for measuring the amount of fluid retained in the corner and the width of the flat region of the prewet film. . . . .	31
5.7	Ca number of ethylene glycol based on the front meniscus and the ratio of the slug length to the radius. . . . .	33
5.8	Ca number of ethylene glycol based on the rear meniscus and the ratio of the slug length to the radius. . . . .	33
5.9	The different energy dissipation zones present in bislug system based on the data collected from the front meniscus. . . . .	34
5.10	The different energy dissipation zones present in bislug system based on the data collected from the rear meniscus. . . . .	34
5.11	. . . . .	35
6.1	Recirculation caused by faster centerline velocity relative to the menisci, faster velocity is required to satisfy the conservation of mass for the system. . . . .	39
A.1	Corner flow captured using a LSCM. . . . .	43

## LIST OF TABLES

3.1	Test parameters for ethylene glycol and silicone oil in circular and noncircular microchannels, the round channel has a radius of 0.469 mm and the square has a hydraulic radius of .5 mm. . . . .	13
4.1	Parameters for Round graphs . . . . .	15
4.2	Parameters for Square graphs . . . . .	18
4.3	Coefficients for $F_{drag}$ in the square channels . . . . .	24
C.1	Coefficients for $F_{drag}$ in the square channels . . . . .	57

# 1. INTRODUCTION

Research for this paper focused on the behavior of a system consisting of two immiscible fluids in a microchannel. The original goal of the project was testing the feasibility of a micropump using the spontaneous capillary motion of the two immiscible fluids. After the micropump was found to be feasible to scope of the research changed to the study of dissipation mechanism in microchannels.

## 1.1 *bislug Definition*

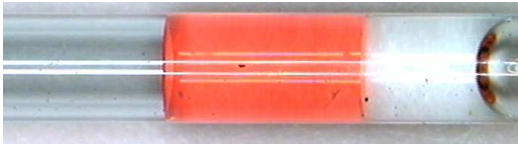


**Figure 1.1.** Bislug in a round microchannel, the dyed liquid is ethylene glycol and the non-dyed fluid is silicone oil.

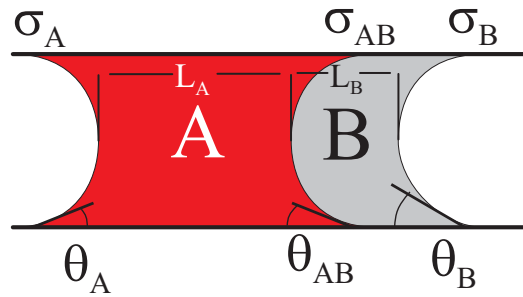


**Figure 1.2.** Schematic of a bislug.

A bislug is defined as two slugs of immiscible liquid in contact in a microchannel. Figure 1.1 is an image of a bislug in a round channel, the darker fluid is ethylene glycol and the light-colored fluid is silicone oil. The subscripts used in the discussion are based on the definitions from Figure 1.2, the front liquid will be labeled “A” and the trailing liquid “B”. Slug lengths are measured at the center of one meniscus to the other. Properties at the different interfaces are labeled “A” for air-liquid A, “B” for air-liquid B, and “AB” for the liquid-liquid interface. A pressure potential is created over the menisci due to a change in the surface tension, a description of the mechanisms for spontaneous flow can be found in the Background, Chapter 2. The bislug flows in the direction from right to left relative to figures 1.1 and 1.2.

## 1.2 *Motivation*

### 1.2.1 *Passive Micropump*

The original goal of the research was a feasibility study for the design of micropump using the properties of a bislug system. The pressure potential from the bislug can

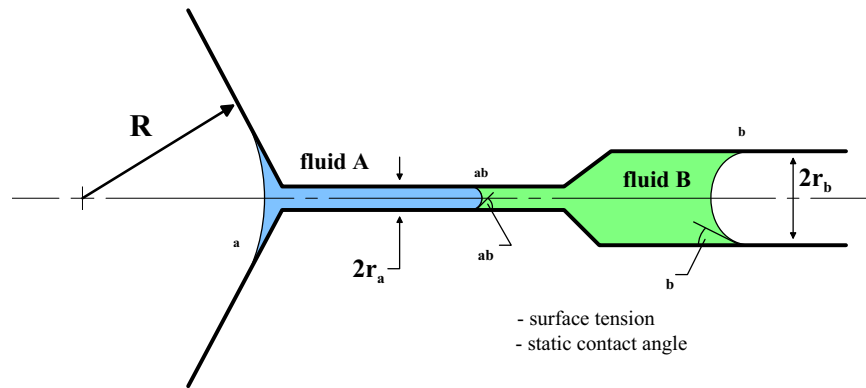


**Figure 1.3.** Schematic of passive pump

be balanced by manipulating the geometry of the channel, see figure 1.3. Chapter 2 has an in depth discussion of spontaneous flow in microchannel. A passive pump is created by the tapered endpiece of the channel. The leading slug will change its radius of curvature until the pressure potential is balanced and the flow is stopped. If fluid is drained from the cone the radius of curvature is changed and the bislug will move to the balanced position. It has been seen from experiments that the response in a round channel may be too slow for a proper fluid pump. A square channel, because of the geometry, may provide for a faster response time, resulting in a feasible micropump.

### 1.2.2 Energy Dissipation

The constant pressure potential created from the bislug may provide an ideal way for studying dissipation mechanisms in a microchannel. From test to test the pressure potential will remain constant as long as the channel and fluid properties remain constant. There are four main dissipation mechanisms in a microchannel; viscous shear, contact line dissipation, menisci interaction and the energy associated with stretching an interface. Interface stretching is included as an energy term in this work due to the properties of the bislug, more discussion in the Chapter 2 and Chapter ???. A model based on the viscous drag and the interface stretching has been developed for predicting the velocity of a bislug in both round and square microchannels.

## 2. BACKGROUND

### 2.1 Capillary Systems

Spontaneous flow of bislugs occurs in microchannels, where the gravitational affect on the interface shape is minimized. The capillary regime will be discussed in detail to bring the reader up to speed. A common example of capillarity is a simple capillary tube placed in a container of fluid. Because of a pressure imbalance at the meniscus the fluid will rise in the channel, if it is wetting, or recede if the fluid is non-wetting, Figure 2.1.

To determine whether the system is in the capillary range, where gravitational affects on the interface are minimal, the Bond number is used. The Bond number is the ratio of gravitational to surface tension forces.

$$Bo \equiv \frac{\Delta\rho g L^2}{\sigma} \quad (2.1)$$

where  $\Delta\rho$  is the density difference accross the meniscus,  $\sigma$  is the surface tension of the meniscus, and  $g$  is the local gravitational acceleration.

A useful variation of the Bo number is the capillary length or Laplace contant,  $L_c$ . The Laplace constant is found by setting the Bo number equal to one and solving for the characteristic length,  $L_c = \sqrt{\sigma/\rho g}$ . This length is the transition between surface tension and gravity dominated systems. A  $Bo \ll 1$  is often used to describe systems where gravity can be ignored when describing the interfacial shape. Though the interfacial shape of the system may not be affected by gravity, **gravity is still**

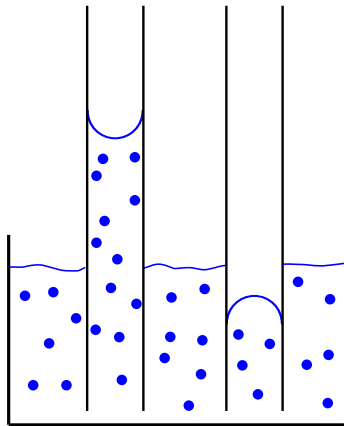


**Figure 2.1.** A wetting fluid rises in a capillary while a non-wetting fluid will recede

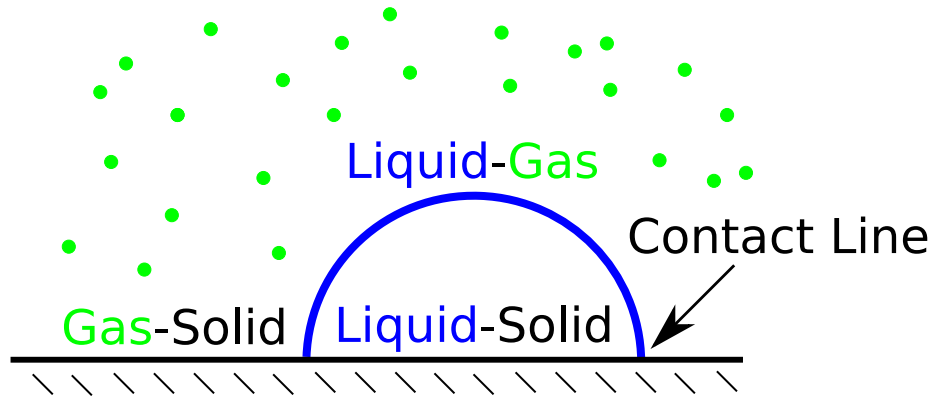


**Figure 2.2.** Configuration of a liquid drop on a solid surrounded by a gas, the intersection of the three materials create the contact line.

**acting on the entire body.** A common misconception is the bulk system is not affected by gravity but a couple of examples will prove otherwise. First, a drop from a cloud or a faucet can easily have a  $Bo \ll 1$  but it will still fall towards the earth. Second, a sponge has pores that are in the capillary range for water and water will wick into the sponge which results in a partially saturated sponge having the bulk of the water at the bottom due to gravity.

Interfacial shapes in a capillary system are dominated by the surface tension of the fluid(s). Surface tension,  $\sigma$ , is the molecular cohesion forces acting at the interface between two fluids and is unique for a given fluid pair. The interfacial shape is determined by surface tension, a surface energy, which tries to minimize the overall surface area, this produces a spherical shape in simple configurations, figure 2.2. The shape of a fluid on a solid surface is a function of the interaction at the contact line. For simplicity, a drop of liquid will be placed on a solid with a gas as the surrounding fluid, Figure 2.2. The contact line is the intersection of the three materials, gas, liquid and solid. Each of the surface energies, gas-liquid, gas-solid, liquid-gas, determine the final shape of the liquid. At the contact line the interaction is quantified using the contact angle. The contact angle,  $\theta$ , is measured from the solid to the tangent at the surface of the liquid at the contact line, figure 2.3. A liquid is considered wetting if  $\theta < 90^\circ$  and non-wetting if  $\theta > 90^\circ$ .

A pressure differential is caused by the curvature of the fluid's interfacial shape and can be calculated using the Laplace-Young equation.

$$\Delta p = \sigma k \quad (2.2)$$

$k = 1/r_1 + 1/r_2$  Where  $r_1$  and  $r_2$  are the principle radii of curvature, which are normal to the menisci. For a round channel this reduces to  $\Delta P = \frac{2\sigma}{R}$ , where  $R = \frac{a}{\cos\theta}$ ,  $a$  is the radius of the channel and  $\theta$  is the contact angle. For a perfectly wetting fluid,  $\theta = 0$ ,  $\Delta P = \frac{2\sigma}{R}$ . Conclusions about the affect that the material and geometric properties of a channel have on the pressure drop are:

1. The radius of curvature changes with contact angle and radius of the channel

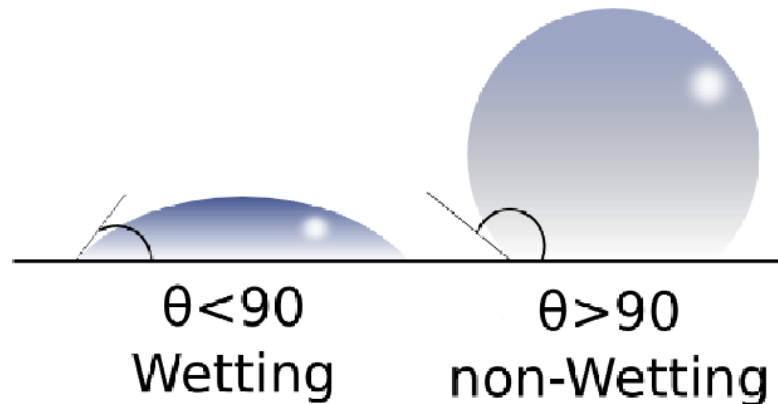


**Figure 2.3.** A wetting system has a contact angle  $< 90^\circ$ , water on clean glass, and a non-wetting system has a contact angle  $> 90^\circ$ , water on wax coated glass.ref

2. Fluids with differing surface tensions will have different pressure drops in the same channel

The pressure drop from the curvature of a fluid is the reason why a fluid will wick into a capillary tube or napkin. The radius of curvature in the capillary,  $R = \frac{a}{\cos\theta}$ , is smaller than the curvature on the surface,  $R \approx \infty$ . This produces a net pressure drop and the fluid is pushed in the capillary until the pushing force is balanced by gravitational forces. Washburn (1921) formulated the first widely reconized predictive equation for the rise time in both a horizontal and vertical oriented channel.

Velocites in microchannels are frequently represented in a non-dimensional form called the Capillary number,  $Ca \equiv \mu V / \sigma$ , where  $\mu$  is the viscosity of the fluid,  $V$  is the velocity of the fluid and  $\sigma$  is the surface tension. The Capillary number is the ratio of viscous forces with surface tension. Velocities can also be represented using the Weber number,  $We = \rho V^2 l / \sigma$ , where  $\rho$  is the density,  $V$  is the velocity,  $l$  is the characteristic length of the fluid and  $\sigma$  is the surface tension. This is the ratio of fluid inertia to surface tension.

Edward, W. Washburn, The Physical Review, The Dynamics of Capillary Flow. 1921 Vol. XVII, No3

## 2.2 Spontaneous Flow

Fluid flow in microchannels is the result of a pressure differential across the length of the channel. Generally the pressure difference is the result of an externally supplied force, for example a channel attached to a syringe pump, constant flow, or a slug of fluid being pushed by a plunger, constant displacement.

Spontaneous flow in microchannels occurs through a pressure imbalance accross the menisci of a slug. Figure 2.4 shows three different configurations that will cause spontaneous motion. Each of which is a manipulation of the Laplace-Young equation 2.2. A difference in surface tension across a slug will cause flow in the direction of the fluid with the highest surface 2.4(a). A change in channel geometry, such as

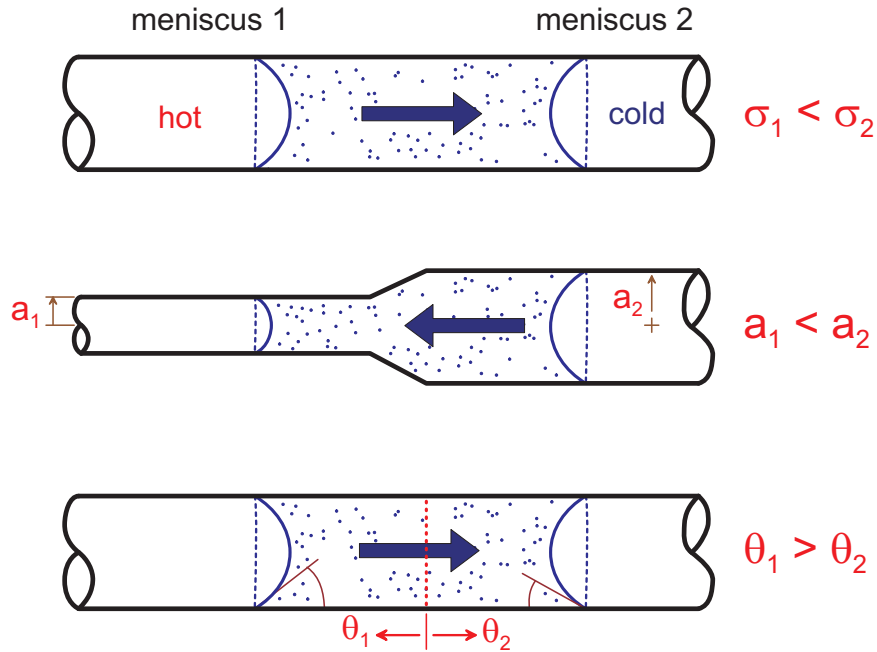


**Figure 2.4.** Spontaneous flow induced in a microchannel from a pressure imbalance caused by a (a) difference in surface tension, (b) change in channel dimensions, and/or (c) change in contact angle.??

an increase or decrease in radius, will change the radius of curvature in the system, which results in flow towards the smaller radius of curvature 2.4(b). Changing the contact angle also changes the radius of curvature, producing flow towards the smaller contact angle 2.4(c).

When two immiscible fluids are in contact, a net pressure drop is produced due to the change in surface tension resulting in spontaneous motion. The motion will be towards the fluid with the highest surface tension. This assumes that the radius of the channel and the contact angles of the two fluids are equal. In the case of differing properties the flow is induced in the direction of the menisci with the largest pressure drop. This phenomenon was first studied in great detail by Bico and Quéré(2002). Their work focused only on bislug flow in round channels, square channels are mentioned during the concluding remarks.

### 2.3 Coating Flows

When two immiscible fluids travel down a channel a thin film of fluid is left on the walls. This can be seen with a classic example of a bubble displacing a fluid in a channel ???. As the bubble moves forward the fluid is pushed out of the channel but leaves behind a thin film of fluid. This film acts a lubricating layer for the bubble to travel on, producing bubbles that travel faster than the liquid film???

Previous research involving coating flows has been directed towards oil recovery enhancement. Water forms a lubricating layer that the oil can travel over, since oil

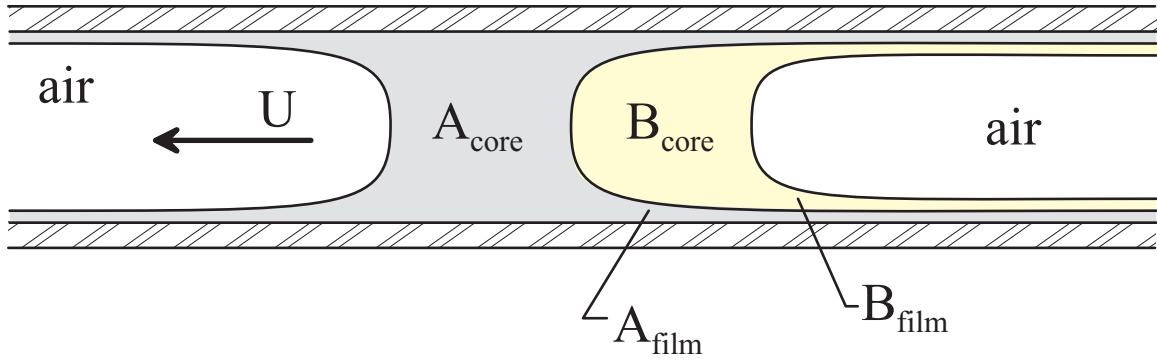


**Figure 2.5.** Schematic of a bislug during flow, both fluids A and B leave a thin film behind.

and water are immiscible they can be easily separated. A comprehensive comparison of data to old and new theory can be found in Bai(1992). Essentially, based on flow rates of the two fluids, different instabilities are formed in the pipes. This is of extreme importance as the amount of energy required changes for the different flow regimes??**Jeff's Paper**. Any increase in energy requirements to push the fluids would mean a large increase in expenditure for oil recovery, due to the large volumes of water used??. An empirical formula for the film thickness was developed by Bretherton (1961),

$$h/r = .634(3Ca)^{(2/3)} \quad (2.3)$$

, the film thickness can be estimated by knowing the Ca number of the system and radius of the channel.

Bislug flow produces a constant pressure drop over the meniscus only, the film does not experience a pressure potential from the menisci. This differs from common annulus flow experiments, where a pressure drop is supplied to both fluids. If the pressure is supplied over the entire radius of the channel the film experiences an external force, which produces flow. As a bislug travels down the channel it leaves a film of fluid A which fluid B travels over, figure 2.5. The film left by A subjected to drag from core B, and the fluid is dragged along, similar to Couette flow. Fluid B also deposits a small film over the film of fluid A. Solutions for the flowrate for both cases can be found in BOOK. The flowrate was in final form for the Couette film flow and could not be used for this study.

F. P. bretherton, Motion of Long bubbles in tubes, J, Fluid Mech. (1961), 10: 166-188

Middleman, Stanley, Modeling Axisymmetric Flows: Dynamics, Films, Jets, and Drops, Academic Press, San Diego,1995. Developes a model for pressure driven annular flow, has flow rationship for film being sheared out of the channel, no useful

Lubricated pipeling: stability of core-annular flow. Part 5. Experiments and comparison with theory, J. Fluid Mech (1992) vol 240 pp 97-132, Runyuan bai, Kangping Chen and D.D. Joseph. Fluid-fluid flow vertical flow, water lubricating oil, oil recovery. Found stability regions for fluid fluid being pumped.

Fairbrother, F. and Stubbs, A.E., 1935. Studies in electroendosmosisVI. The

bubble tube method of measurement. *Journal of Chemical Society* 1, pp. 527529.

Energy Demands on Water resources, Report to Congress on the interdependency of energy and water, December 2006 U.S. Department of Energy.

## 2.4 Corners

To test the feasibility of the bislug micropump, two different cross-sectional microchannels were used. From previous experiments(??) it has been shown that a bislug will flow in round channels. However, square channels, or channels of non-circular cross-sections had not been tested. A uniform film thickness is deposited on the walls of a round microchannel when coated with wetting liquid. A square microchannel exhibits a different form of coating. As a fluid slug traverses a square microchannel it leaves a thin film on the walls similar to the round channels, but it may also deposit a thicker film in the corners, Figure 2.6. Whether or not the fluid is retained in the corners is dependent on the Concus-Finn criteria (?). The criteria for corner wicking is a function of the contact angle of the fluid and the surface,  $\theta$ , and the half angle of the corner,  $\alpha$ , Figure 2.7.

$$\theta \leq \frac{\pi}{2} - \alpha \quad (2.4)$$

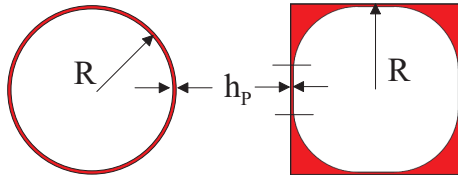


**Figure 2.6.** Coating profiles of liquid films in different channel geometries.

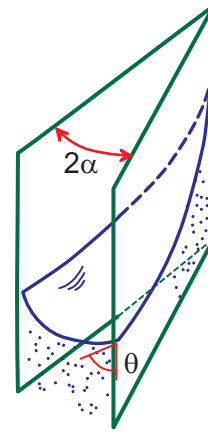


**Figure 2.7.** Spontaneous wicking of a fluid into a corner satisfying the Concus-Finn Criteria.

For the test setup both fluids are perfectly wetting to the glass and the square microchannels have corners with half angles of  $45^\circ$ . For any fluid in a square channel  $\theta \leq 45^\circ$ . Fluids with contact angles between  $45^\circ$  and  $135^\circ$  are partially wetting in square microchannels; that is, the fluid behaves like it would in a round channel. Any channel with corners can have fluid spontaneously wick into the corners if it satisfies the Concus-Finn criteria. The spontaneous flow of the fluid is induced by a difference in curvature. This curvature difference causes a net pressure imbalance in the same manner as Figure 2.4(b). Figure 2.8 represents fluid in a wedge, the wedge is one

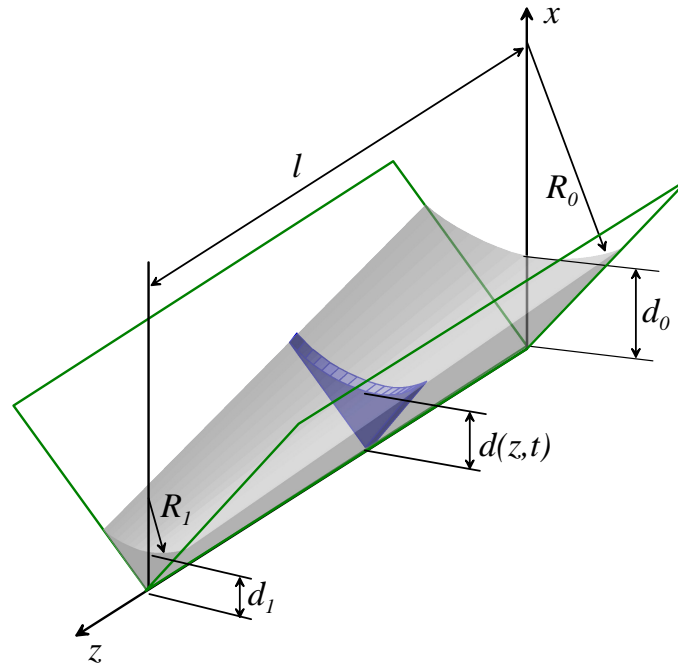


**Figure 2.8.** The schematic of a wedge with spontaneous corner wicking.

of the four corners of a square channel, the radius of curvature reduces from left to right. The reduction in curvature can theoretically occur to infinity, resulting in an infinite flow potential. The smallest radius of curvature is limited by either the scale required to continue coating is smaller than the thickness of a molecule of the fluid or the more likely, a channel defect. The channel defect can be a result of “dirt” in the corner which provides a location to pin and stop the flow or a manufacturing defect, such as rounded corners. The radius of the rounded corner is the smallest radius the fluid can have, limiting the overall distance for the spontaneous flow. The “finger”, fluid displaced from the meniscus, which is produced from the corner flow can be characterized by  $H$  ??  $H$  is the length of the displaced from fluid from the meniscus to the end of the fluid.

Taylor 1961 Cerro Kolb Shape of meniscus, attempts at solving the velocity profile. bubble flow.

Weislogel: Flow in the core. Include some of the writeup. Capillary Flow in an interior corner, Nasa Technical Memorandum 107364, 1996, Mark M. Weislogel Calculated flowrate of fluid in an interior corner, based on geometry of the wedge, calculated a height from the meniscus where the fingers start.

Bubble-Train Flow in Capillaries of Circular and Square Cross section, T. C. Thulasidas, M. A. Abraham, R. L. Cerro. Chemical Engineering Science, Vol 50, No 2, pp 183-199, 1995 Bubble train flow in round and square crosssection monolith reactors, determine optimal flowrates of gas and liquids, bubble size and shape. Good summary of previous work with bubble flow in channels, found a flowrate around the bubbles as long as it was gravity driven

### 3. EXPERIMENTAL SETUP

Video of the bislug was recorded using standard image capturing techniques. A Panasonic GP-KS152 color CCD camera was attached to an optics port on a Nikon SMZ1500 microscope. The microscope was attached to boom stand, a stand that has six degrees of freedom, for course microscope adjustment. The boom stand was setup on a x-y translation stand which allows for fine adjustment in the x-y directions and the microscope focusing adjusted in the z-direction. A video capture card, Epix model PIXCI SV5 , was used to record the image sequences from the camera to a computer. The Epix board had a working frame rate of approximately 30 frames per second(fps). Image files were saved using a .tiff format to retain pixel information which may be lost using other standard image file formats. Capturing of a crisp interface required a fast shutter speed and proper lighting. The shutter speed was set to 1/1000 of a second. A faster shutter speed captures a crisp interface at the menisci reducing the blurring caused by fast slug flow. As the shutter speed increases the amount of light needed also increases. The first attempt at lighting used a ring light attached to the microscope lens. This provided enough light but also produced flares where the light crossed the glass channels. To remove the flares diffused light was used, this required a transmitted illumination setup. For the diffused lighting the channel test fixture was made from glass. Microscope covers were glued onto a microscope slip with enough space to set the microchannel into place. Using this setup the alignment of the microchannels could be maintained for all test runs; the microchannels were placed in the same direction and maintained the same focal distance. Also, the scaling was kept constant between test runs because the magnification was not changed. Images of the experimental setup can be seen in Figures 3.1, 3.2.

Ethylene glycol and silicone oil were used for the immiscible fluid pair. These are the same fluid pair used by Bico (?) in the original bislug experiments. Properties for the fluids were taken from Bico (?) and are listed on Table 3.1. For better contrast, the ethylene glycol was dyed using red food coloring, which is a mixture of coloring, propylene glycol, and water. Only a small amount of coloring was used to minimize the affect the food coloring would have on the ethylene glycol properties. The silicone oil was not dyed because the contrast between the ethylene glycol and silicone oil was sufficient enough for image processing.

Round and square micro-channels made from borosilicate glass were used for the test sections. These channels were chosen to be consistent with previous work and the fluids are perfectly wetting to the glass; therefore the low contact angle satisfies the Concus-Finn criteria for square microchannels. The round microchannels are  $40\mu L$  yellow band disposable pipets manufactured by Drummond Scientific. The channels are drawn with an average inner diameter of approximately 0.938 mm, which was



**Figure 3.1.** Experimental setup.

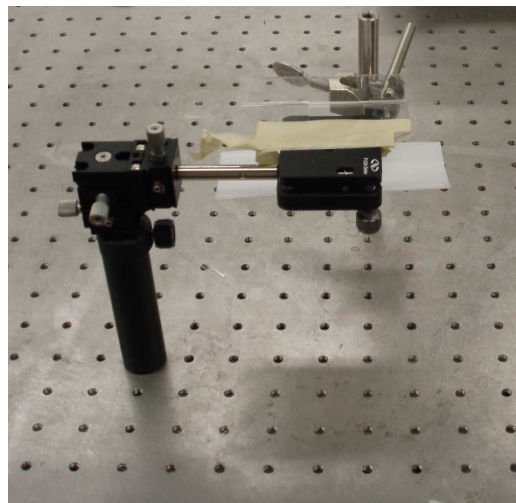


**Figure 3.2.** Bislug test fixture.

calculated from knowing the volume and calibrated fill length of the channel. The square channels had an inner side dimensions of 1 mm square and were manufactured by Vitrocom. Microchannels with hydraulic diameters close to 1 mm were chosen for optical clarity. As the channel diameters decrease a higher magnification is needed to view the menisci, the higher magnification decreases the viewable working area of the microchannel. A large working area is preferred to increase the amount of time the bislug remains in the field of view. This decreases the amount of error in the data processing. Smaller diameter channels also produce longer slugs than large diameter channels for the same fluid volume which creates difficulties when trying to control slug lengths.

The bislug was created using two different methods. To create the bislug using the first method, a channel was dipped into a vial containing ethylene glycol. Ethylene glycol was drawn into the microchannel by capillary forces. To prewet the channel, the tubes were inverted and gravity pushed the slug of ethylene glycol down the channel; thus coating the channel walls with a film of liquid. The slug of ethylene glycol could be adjusted by wicking some fluid out using a paper towel. The prewet channel was then dipped into the silicone oil allowing capillary forces to draw fluid in. Keeping the channel vertical prevented long slugs of silicone oil from forming, the length of silicone oil depended on the length of the ethylene glycol, to increase the length of either slug the channel could be tilted, positioned between vertical and horizontal, to reduce the effect of gravity. For test runs requiring nonprewet channels, the ethylene glycol slug was inserted into the silicone oil vial after adjusting the slug length. After the bislug was formed the microchannel was set onto the test setup.

A second method, for generating bislugs used syringes to accurately control the lengths of the slugs. Thin needles were attached to both push and screw style syringes. The screw style provided tighter control over the volume being inserted. Ethylene glycol could be accurately deposited in the microchannels but prewetting the system was difficult. To prewet, the channels had to be removed from the setup, turned vertical and realigned after the prewetting was complete. Longer slugs, when tipped vertical, would drain because the force of gravity was larger than the capillary forces. To make longer slugs the microchannel was filled with a small slug and inverted to wet, the microchannel was realigned and the syringe was used to increase the size of the slug. After injection of the ethylene glycol a syringe with silicone oil was used to create the bislug. This procedure, though more precise, was not practical due to the spontaneous nature of the bislug flow. As soon as silicone oil was deposited the bislug began to flow. This prevented the deposition of long silicone oil slugs. Bubbles could also be trapped in the system due to the shape of the meniscus. Without gravity pushing the slug down, like in the previous method, the meniscus was curved which created a gap between the meniscus and the microchannel end. In a square microchannel the ethylene glycol would migrate down the channel to balance the pressure gradient caused by the corner flow. This did not allow for the silicone oil to be deposited without an air bubble. Different techniques were attempted to prevent the bislug from moving, but each attempt was unsuccessful. This technique proved to be too cumbersome and the first method was used.

Spotlight, an image tracking software developed at the NASA Glenn Research Center by B. Kilmek and T. Wright, was used for measuring the bislug systems (?). An interface tracking Area-of-Interest(AOI) was setup to track both the front and rear menisci. Lines produced by the NTSC video were smoothed to produce an average interface and a low pass filter was used to create a sharp tracking edge. The software recorded the change of position with time, values for the length and framerate were used for scaling. Spotlight outputs an ascii file containing the information regarding scaling and the values from the tracking AOI. These text files were imported to Lotus 123, Excel, and MATLAB for data processing. Acceleration and velocity of the bislug were determined by using a least square polynomial fit of the position and time. Errors from the data collection were determined to be  $\pm 2$  pixels for the length measurements and  $\pm 2$  fps for the time measurement. The value of 2 pixels is the measurement error for the length of a slug. Measurements in Spotlight are accurate to a pixel in both the x and y directions, the decimal values are from the norm of the components. Video captured using the CCD camera is interlaced, half of the frame updates every  $1/(2\text{fps})$ , this value was chosen for the error that can occur between frames.

Inconsistencies in both the prewet and dry data may be attributed to the quality of the microchannel used. The round and square microchannels are manufactured by drawing glass over a mandrel. Imperfections in the process can produce channels with fluctuations in the radius over the length of channel, these fluctuations will cause a change in the instantaneous velocity. This process also produces square channels with rounded corners, this limits the pressure developed in the corners from the spontaneous fluid flow.

**Table 3.1.** Test parameters for ethylene glycol and silicone oil in circular and noncircular microchannels, the round channel has a radius of 0.469 mm and the square has a hydraulic radius of .5 mm.

parameter	ethylene glycol (A – air)	silicone oil (B – air)	(A – B)
$\nu$ [cSt]	16	1	
$\Delta\rho$ [kg/m <sup>3</sup> ]	1113	963	150
$\mu$ [kg/ms]	0.0178	0.0096	
$\sigma$ [mN/m]	47.7±0.1	20.3±0.1	18.0±0.2
$L_c$ [mm]	2.09	1.47	3.50
Bo	0.050 - 0.057	0.10 - 0.12	0.018 - 0.020

## 4. NUMERICAL MODELING

Numerical modeling of the bislug system was performed in two steps. First, the flow profiles for fluid A and fluid B were determined. The velocity at the transition from film A and core B was also found. Second, an integration of the shear stress over the surface area in which it acts found drag force in the three flow profiles.

To model the flows in both the round and square channels common flow profiles were assumed. For the core the slugs, where the menisci pressure potential acts, a classic Hagen-Poiseuille flow profile was assumed. A Couette flow profile was used for the film. This was chosen due to the only motion that produces the flow was in the core. A boundary of equal velocity and shear was used for the transition from the core to the film. Figure 4.1 shows the profiles used for the core and the film,  $U_{AB}$  is the velocity at the transition and  $U_{max}$  is the centerline velocity. The full derivation for the round channels is in Appendix B and the square channel derivation is in Appendix C.

### 4.1 Velocity Profiles

#### 4.1.1 Round

As mentioned above a Hagen-Poiseuille flow was used in the core and a Couette profile was used in the film. The boundary conditions used were: no-slip at the wall, a line of symmetry in the core, and a no-slip condition at the film. When a film is not present, the case for the front slug, a Hagen-Poiseuille profile was used over the entire channel width. Solutions for the velocity profiles are presented below, see Appendix B for the full derivation:

$$u_{CoreA} = U_{max} \left[ 1 - \left( \frac{r}{R} \right)^2 \right] \quad (4.1)$$

$$u_{FilmA} = U_{AB} \frac{\ln \left( \frac{R}{r} \right)}{\ln \left( \frac{R}{R-h_A} \right)} \quad (4.2)$$

$$u_{CoreB} = (U_{max} - U_{AB}) \left( 1 - \frac{r^2}{(R-h_A)^2} \right) + U_{AB} \quad (4.3)$$

where

$$U_{AB} = \frac{U_{max}}{1 + \frac{1}{2} \frac{\mu_A}{\mu_B} \frac{1}{\ln \left( \frac{R}{R-h_A} \right)}} \quad (4.4)$$

The solution for the velocity in the thin film, equation 4.2, matches the solution from previous derivations of concentric cylinders with the inner cylinder moving??white's

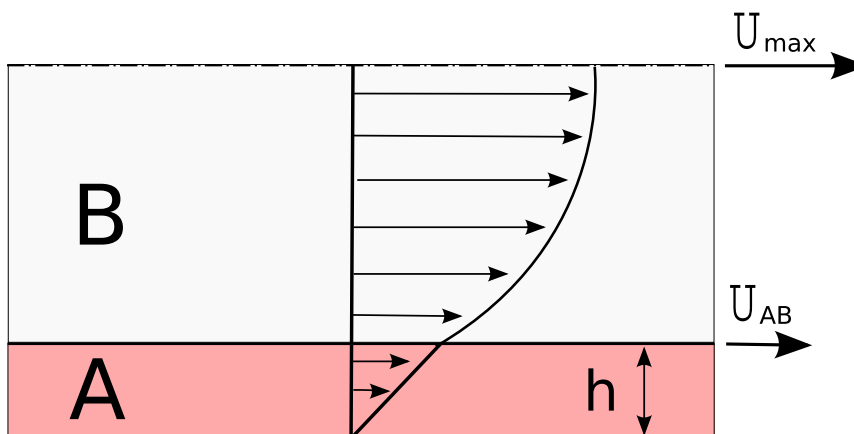


**Figure 4.1.** Assumed flow profiles of the Core and film used in the derivation of the models.

book. Since the boundary conditions were no slip at the transition between the film of fluid A and core of fluid B the equation for the transition velocity contains elements of both profiles and introduces a logarithmic term to the Hagen-Poiseuille profile. For modeling purposes the domain was examined at the upper and lower limits for the Ca number of the experimental data because the film thickness is calculated using the equation 2.3 . Both the flow for the prewet and dry test runs were modeled using the derived equations.

**Table 4.1.** Parameters for Round graphs

Test Runs	Ca	$U_{max}(mm/s)$	$h_o(\mu m)$
Dry Round Low Ca fig 4.2(a)	4E-5	0.1072	0.7822
Dry Round High Ca fig 4.2(b)	2E-4	0.5360	2.2871
Prewet Round Low Ca fig 4.4(a)	2E-4	0.5360	2.2871
Prewet Round High Ca fig 4.4(b)	3E-4	0.8039	2.9969

Flow profiles for both the dry and prewet channels are presented in figures 4.2 and 4.4, respectively. The flow profile for Core A (no-immiscible film) and Core B/Film A are plotted on the same graphs. The channel radius is non-dimensionalized using  $\zeta = r/R$ , where R is the radius of the channel and r is the current position relative to the center of the channel. The x-axis is the non-dimensional velocity,  $U/U_{max}$ , where  $U_{max}$  is the centerline velocity and U is the calculated velocity at position r. Table 4.1 has the information for each test run.

Both flow profiles appear to overlap oneanother for each graph and its not until the magnification is increased near the wall that the divergence appears, figures ?? and 4.5. Couette flow in the film has little effect on the overall flow profiles. The films, calculated from the Bretheron (1961) relationship, are small compared to the radius and the natural log term for  $U_{AB}$  and  $u_{FilmA}$  is approximately zero.

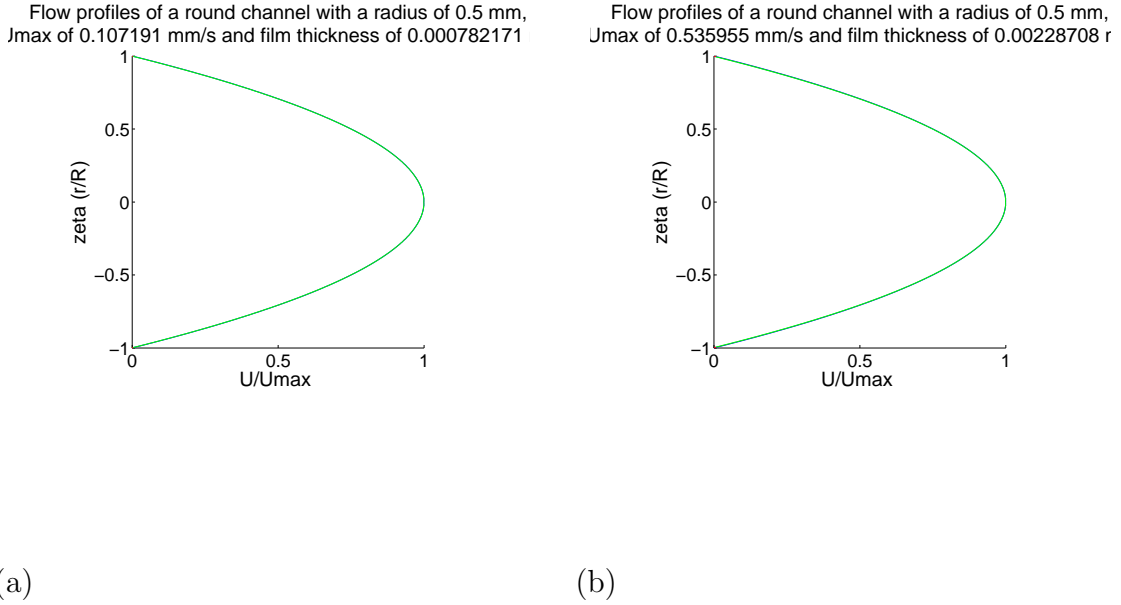


**Figure 4.2.** Flow profiles for the dry channels.

#### 4.1.2 Square

Relationships for the velocity profiles in the square channels were found in the same manner as the round channel. The same equations were used for the solution of the round channels with the exception of the radius term. A relationship for the distance from the center of the square channel to any point was used, producing a sudo radius term,  $s$ .

$$s = \sqrt{x^2 + y^2} \quad (4.5)$$

Using  $s$  for the radial term the equations for the velocities in the square channels are:

$$u_{CoreA} = U_{max} \left[ 1 - \frac{s^2}{S_o^2} \right] \quad (4.6)$$

$$u_{FilmA} = U_{AB} \frac{\ln\left(\frac{S_o}{s}\right)}{\ln\left(\frac{S_o}{S_f}\right)} \quad (4.7)$$

$$u_{CoreB} = (U_{max} - U_{AB}) \left( 1 - \frac{s^2}{S_f^2} \right) + U_{AB} \quad (4.8)$$

$$U_{AB} = \frac{U_{max}}{\left( 1 + \frac{1}{2} \frac{\mu_A}{\mu_B} \frac{1}{\ln\left(\frac{S_o}{S_f}\right)} \right)} \quad (4.9)$$

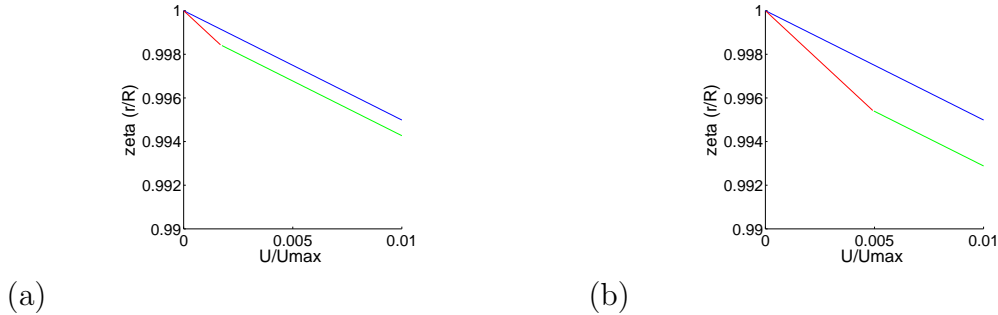


**Figure 4.3.** zoomed flow profiles for the dry channels.

Full derivation of the equations are in Appendix C.

Velocity profiles for the square channels were calculated at varying points along the channel due to the dependence of the equations on two variables. The position on the wall was held constant at various points and the other variable was varied over the test range. Figure 4.6 has the geometry of the square channel used for the calculations. The channel consists of eight symmetric regions, the models use a single region shown in the right picture in figure 4.6. The schematic shows the distances in non-dimensional form,  $\sigma = s/R$  where  $R$  is hydraulic radius of the channel, half of the wall length for a square. The o and f subscripts indicate the distance to the wall and the transition from film to core, respectively. The transition is broken into two parts, the flat region has film thickness of  $h_o$  and the corner has a radius of  $R_c$  and a film thickness of  $h_c$ .

Plots of the slug profiles are split between the lead and trailing slugs due to the amount of information presented. Profiles for the leading slug are plotted in figure 4.11 for the high Ca number and figure 4.16 for the low Ca number. Each of the figure sets consists of the flow in Core A (without film), Core B and Film A, the location of the profiles in the channel and the velocity of the transition. The non-pretwet channel was not modeled because of the erratic data obtained during experimentation. Because of the corner flow the channel is never truly dry and amount of fluid pumped into the corners depends on the time between the trailing slug introduction, channel defects, and channel orientation during experimental setup. Both the profiles in Core A and Core B/Film A have the same general shape but the effects of the film can be seen clearly which differs from the round channels where the Couette flow had little effect. Since the film was a constant height in the flat region the solutions for the profiles are merely stretched or elongated from profile to profile in the direction from the center to the wall until the transition into the corner. The film velocities are no longer constant in the corner due to the changing film thickness which is now dependent on the profile's position in the channel. If the Concuss-Finn criteria had not been met then the film thickness would remain constant along the channel. The films were calculated using the Bretherton relationship, the increase effect from the Couette flow may be attributed to the order of magnitude increase in Ca number from round pretwet to square pretwet.

From the pressure differential caused by the geometry fluid is pumped into the

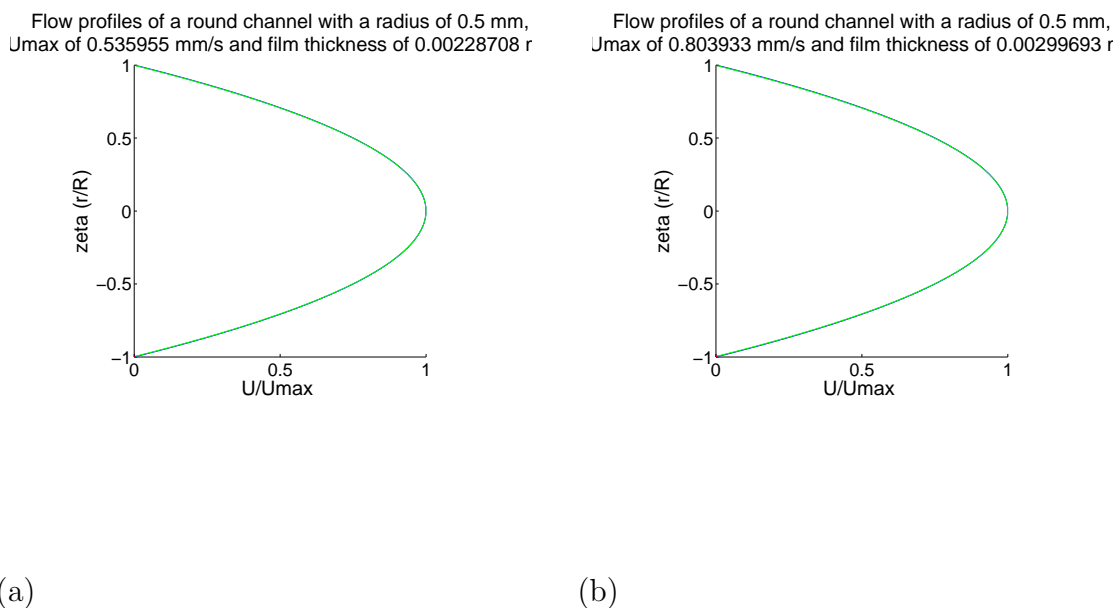


**Figure 4.4.** Flow profiles for the prewet channels.

**Table 4.2.** Parameters for Square graphs

Test Runs	Ca	$U_{max}$ (mm/s)	$h_o$ ( $\mu\text{m}$ )
Prewet Square Low Ca (a)	2E-3	5.3596	10.615
Prewet Square High Ca (b)	4E-3	10.7191	16.851

corners away from the meniscus. This pumping changes the flow profiles in the film. A complex flow profile is produced from the interaction of Hagen-Poiseuille profile produced from the corner pumping and the Couette profile formed from the drag. For the front meniscus the two are flowing in the same direction while the trailing slug has Couette flow in the direction of bislug and pumping in the opposite direction. Weislogel has a derivation for calculating the flowrate from the meniscus in the corners and will be added into the flow equations in later work.

The radius of the film in the corner was estimated to be 10% of the channel width based on figure 5.6 in Chapter 5. Kolb developed a relationship for calculating the radius but the properties for this setup resulted in a negative number. Kolb used higher flowrates which results in Ca numbers that are larger than those in these experiments. Also, the extrapolation of the presented graph also results in a negative number for the low Ca numbers.

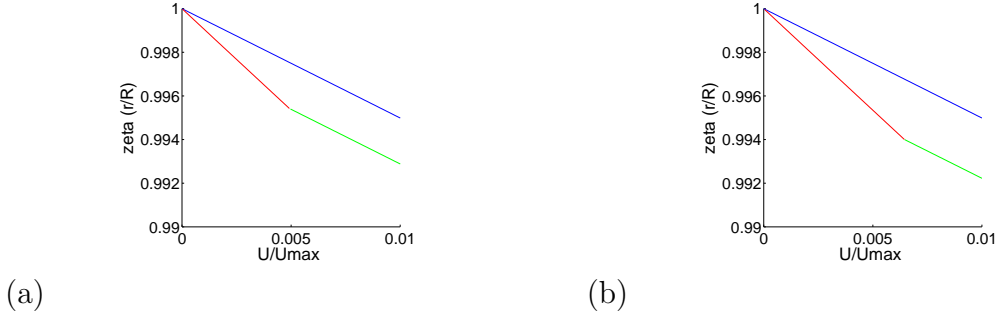


**Figure 4.5.** zoomed flow profiles for the prewet channels.

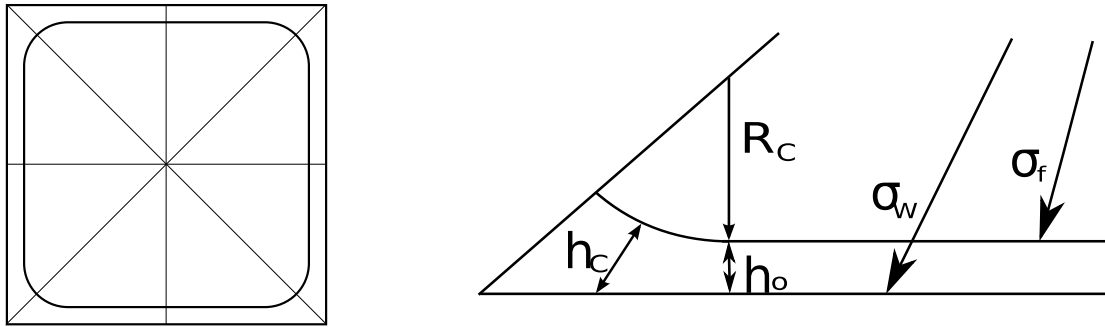


**Figure 4.6.** Geometry for the square channels. The square profile has eight symmetric sections, each of the sections has the profile on the right

## 4.2 Force Balance

### 4.2.1 Round

The force balance is the summation of the pressure force, drag force and interface stretching terms. The pressure potential is calculated using the Laplace-Young equation 2.2 and the force can be calculated by multiplying this over the area of the menisci. The drag force is the result of the shear stress and is applied to the surface area in which it acts. The interface stretching term is the result of the destruction and creation of the thin films as the bislug moves down the channel. Bico and quere used it to justify that the pressure potential resulted from the surface tensions, it is included in this work as a term that adds and removes energy from the system.

To study the dissipation mechanisms present in slug flow a model based on the force balance between the pressure potential, drag force and the energy needed to stretch the interface in the area near the menisci has been developed. The pressure potential of a bislug system is dependent on the differences in surface tensions of the three interfaces and the radius of the channel (equation 4.10).

$$\Delta P = \frac{2(\sigma_A - \sigma_{AB} - \sigma_B)}{R} \quad (4.10)$$

The net drag force is comprised of three separate components: (i) the drag in the core of slug A, (ii) the drag in the core of slug B, and (iii) drag in the thin film of fluid A

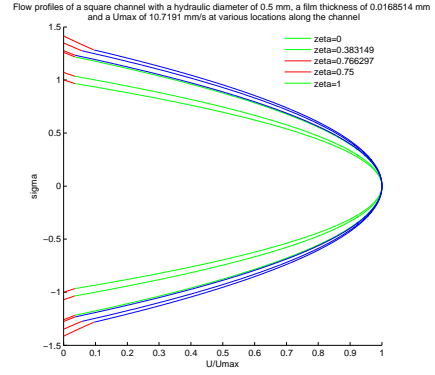
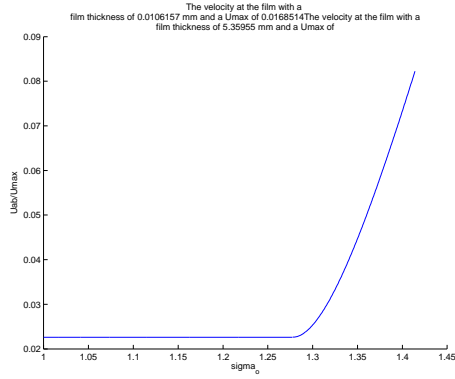


**Figure 4.7.** high- profiles without films

**Figure 4.8.** high-profiles with film

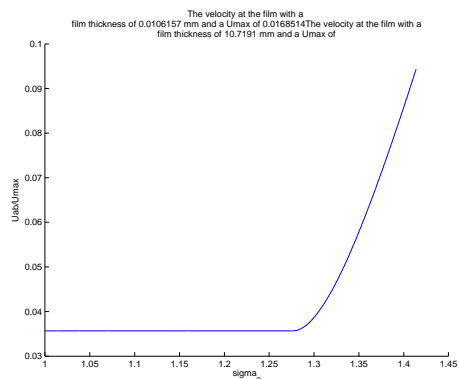
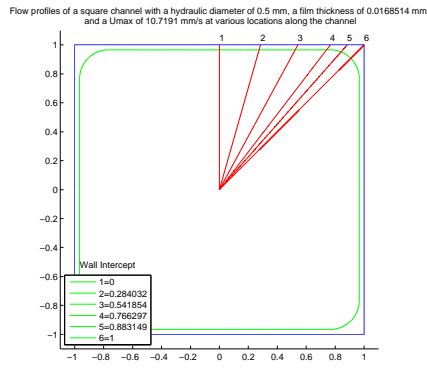


**Figure 4.9.** high-Prewett flow profiles lines

**Figure 4.10.** high-film velocity

**Figure 4.11.** High Ca Number profiles

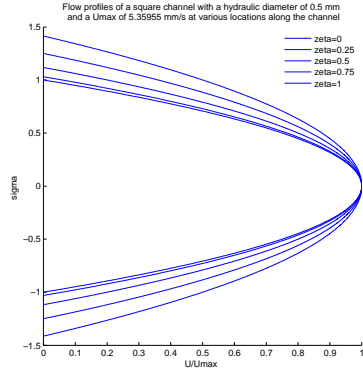


Figure 4.12. low-profiles without films

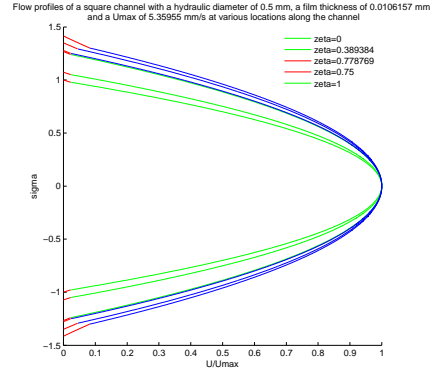


Figure 4.13. low-profiles with film

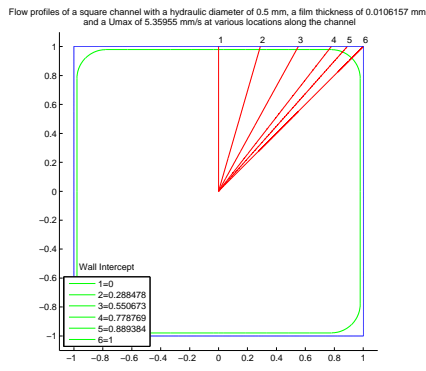


Figure 4.14. low-Prewett flow profiles lines

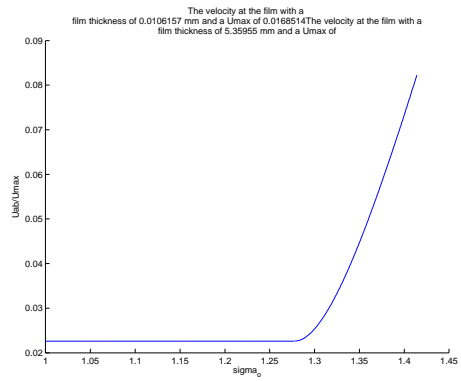


Figure 4.15. low-film velocities

Figure 4.16. Low Ca Number profiles

that is under slug B. A thin layer of ethylene glycol, fluid A, is deposited on the walls of the microchannels before fluid B is introduced for prewet test runs or a thin fluid is deposited over the dry channel as the bislug traverses the channel. Since fluid A and fluid B are immiscible the thin film of fluid A remains intact under the slug of fluid B. Flow in both the cores of slug A and slug B are model as Hagen-Poiseuille flow due to the constant pressure potential between the menisci. Couette flow was assumed for the thin film; there is a no slip condition at the wall and a constant velocity at the interface between film A and slug B. The total drag force is the sum of all three of these components.

$$F_{drag} = F_{coreA} + F_{filmA} + F_{coreB} \quad (4.11)$$

The resulting equation for the drag force is equation 4.12,

$$F_{drag} \approx 4\pi\sigma_A L_A Ca_A \left[ 1 + 2\frac{1}{M} \left( \frac{L_B}{L_A} \right) \right], \quad Ca \leq 10^{-3} \quad (4.12)$$

where the velocity has been non-dimensionalized using the Ca number for the leading slug,  $Ca_A = U_{max}\mu_A/\sigma_A$  and M is the viscosity ratio,  $\mu_A/\mu_B$ . The full derivation can be found in Appendix B.

As a bislug of fluid travels down a prewet microchannel, the front meniscus destroys the thin film, prewet air-film A interface; absorbing energy. At the same time meniscus AB and meniscus B create new interfaces on the wall, which requires energy and reduces the overall potential for flow in the system. Flow in a single slug has only two menisci. The amount of energy restored from the destruction at the front meniscus is removed with the creation of the interface at the rear meniscus for a net energy creation or destruction to be approximately zero. In a bislug system there are three different surface tensions at the different menisci resulting in a non zero energy exchange. For this setup there are two interface creations and one destruction which, depending on the surface tensions, produces a net energy change in the system. Equation 4.13 is the final form of the solution and it is based on the summation of the three stretching terms across the the bislug.

$$F_{stretch} = \sigma P_{e,coat} = 2\pi R \left[ \left( 1 - \frac{h_A}{R} \right) (\sigma_{AB} + \sigma_B - \sigma_A) - \sigma_B \frac{h_B}{R} \right] \quad (4.13)$$

where  $P_{e,coat}$  is the perimeter of the film cross-section. Equation ?? is the final form of the model and has been non-dimensionalized using the Capillary number. The full derivation can be found in Appendix B. From the model it can be seen that the Capillary number is a function of the surface tensions of the two fluids, the radius of curvature, and the lengths of the slugs. The final form of the model is equation 4.14.

$$Ca_{max} \approx \left[ 1 - \left( \frac{\sigma_{AB} + \sigma_B}{\sigma_A} \right) \right] \left( \frac{R}{L_A} \right) \left( \frac{1}{1 + 2\frac{\mu_B}{\mu_A} \frac{L_B}{L_A}} \right), \quad \text{for } Ca < 10^{-3} \quad (4.14)$$

The drag force in round channels has been solved for the Core B and Film A as a function of film thickness. Values for the drag force are the coefficient multiplied by the centerline velocity and the slug length. Both the drag from the film and core

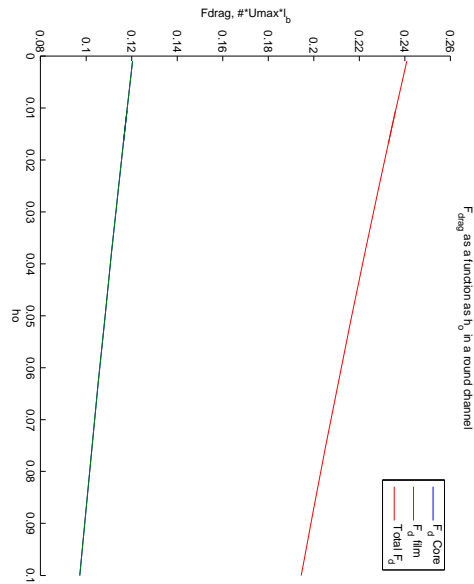


**Figure 4.17.** Drag forces in a round channel, because of the small change in surface area the drag forces overlap.

plotted one the figure, left plot in figure 4.17. The values overlap showing that the amount of drag of in the core is dependent on the amount of shear in the film, which is dependent on the shear stress on the the wall. The shear stresses are equal because it was assumed that the local shear stresses of the core and film at the transition are equal. The areas that the shear stresses act over are approximately the same due to the small film thickness, resulting in the same shear stress numerically.

#### 4.2.2 Square

The summation of forces in a the square channels used the same approach as the round. A balance between the motive, drag and stretching forces was used. Though the channel is square the menisci of the slugs have a sperical shape, this produces the same pressure potential resulting in teh same equation as the round channels, equation 4.10. Where R is the hydraulic radius, which for a square is half of the side wall length.

As with the round geometry the square channels also have interface destruction and creation as the bislug travels down the channel. Each of the menisci have a two

part profile, a flat and curve section, figure 4.6.

$$F_{stretch} = 8(F_{stretch_{flat}} + F_{stretch_{corner}}) = 8\sigma(Pe_{flat} + Pe_{corner}) \quad (4.15)$$

The multiplier of eight is used because the channel was broken into eight symmetric parts, figure 4.6. The final form of the stretching term is

$$2\pi R \left[ \left(1 - \frac{h_A}{R}\right) (\sigma_{AB} + \sigma_B - \sigma_A) - \frac{x_f}{R} (\sigma_{AB} + \sigma_B) - \sigma_B \frac{h_B}{R} \right] + 8x_f(\sigma_{AB} + \sigma_B) \quad (4.16)$$

The full derivation is in section C.1.1 of the Appendix.

The summation of the forces for the square channels does not result in a closed form solution like the round channels. The drag term requires numerical integration for solution due to the complex form of the shear stresses. The term that is numerically integrated is dependent on the viscosity ratio which depends on the system properties. Results for the drag are unique for each fluid pair. Equations for the drag in the three regions of bislug are below. The results for the drag in Film A and Core B are combined and the numerical value from the integration is contained in the variable  $\alpha$ . A closed form solution is available for Core A but the variable  $\beta$  was used to keep the equations consistent. Table 4.3 has the coefficients from the integration at the two boundary Ca numbers. The drag force in the channels decrease as the film thickness increases, figure 4.18. This is expected because the simple form of the shear stress in the film is dependent on the thickness of the film. Differing from the round geometry there is a clear separation between the shear stress in the film and the fluid core. This is due to the change in geometry from the flat film to the corner, which decreases the active area for the shear stress in fluid B to act over.

$$\begin{aligned} F_{drag_{CoreA}} &= \beta\mu_A U_{max} L_A \\ F_{drag_{CoreB}} + F_{drag_{FilmA}} &= \alpha U_{max} L_B \end{aligned} \quad (4.17)$$

**Table 4.3.** Coefficients for  $F_{drag}$  in the square channels

Ca Number	$h_o$ ( $\mu\text{m}$ )	$\alpha$ (kg/m s)	$\beta$
2 E-3	10.6	0.52567	14.1020
4 E-3	16.9	0.51926	14.1020

The resulting model from the force balance is equation 4.18. The velocity has been non-dimensionalized using the Ca number with respect to fluid A. The film thickness for fluid A,  $h_A$  is approximated from the Bretherton relationship, the film for fluid B

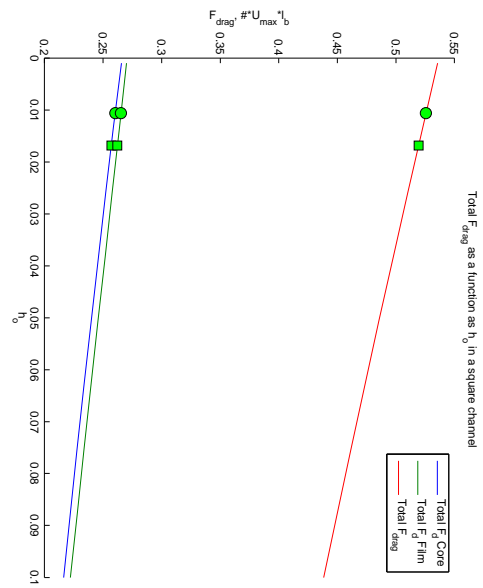


**Figure 4.18.** The drag in a square channel, the circle and square are the boundaries used for data comparison, low  $Ca$  and high  $Ca$ .

was assumed to be close to zero, this has a minimal effect on the model.

$$Ca_{Amax} = \frac{U_m ax \mu_A}{\sigma_A} = \frac{2\pi R \left[ \left( \frac{\sigma_{AB} + \sigma_B}{\sigma_A} \right) \left( 2 - \frac{h_A}{R} \right) + \frac{x_f}{R} \left( 1 - \frac{4}{\pi} \right) \left( \frac{\sigma_{AB} + \sigma_B}{\sigma_A} \right) \right]}{L_A \left( \frac{\alpha}{\mu_A} \frac{L_B}{L_A} + \beta \right)} \quad (4.18)$$

A model was also developed without the inclusion of the stretching term. The results will be used to compare the role of the stretching term.

$$Ca_{Amax} = \frac{2\pi R \left( 1 - \left( \frac{\sigma_{AB} + \sigma_B}{\sigma_A} \right) \right)}{L_A \left( \frac{\alpha}{\mu_A} \frac{L_B}{L_A} + \beta \right)} \quad (4.19)$$

## 5. RESULTS AND DISCUSSION

Bislug flow in round channels was reproduced to verify the work done by Bico (??). Tests used both prewet and dry test runs and were performed in round and square microchannels over various slug lengths.

### 5.1 Round Microchannels

Velocities for both the prewet and dry microchannel test runs were non-dimensionalized using the capillary number with reference to the ethylene glycol (equation 5.1). A non-dimensionalized length scale  $L_A/R$  is used where R is the radius of the channel. For the data discussed  $R=0.469$  mm.

$$Ca = \frac{\mu_A V}{\sigma_A} \quad (5.1)$$

Data from both the prewet and dry test runs are plotted on Figure 5.1. There is a noticeable difference in velocity between the prewet and dry microchannels. Bislug flow in a prewet channel is approximately 2-3 times faster than the dry channel. The average capillary number for dry and prewet tests are  $1 \cdot 10^{-4}$  and  $2 \cdot 10^{-4}$ , respectively. Differences in velocity can be attributed to energy dissipation associated with the dragging of the contact line across a dry surface. A prewet channel has a thin layer of fluid deposited on the walls before the bislug is created as described earlier. This coating reduces the energy dissipation with the moving contact line. In both systems the pressure difference between the two menisci is the same,  $\Delta P = 40.1$  Pa. As such, this type of experiment may provide a way to study energy dissipation near a moving contact line if a proper model can be developed.

Bislug flow was previously modeled as classic Hagen-Poiseuille flow (??). This model, to compare to the model produced in this work, has been non-dimensionalized into equation 5.2.

$$Ca = \frac{\mu_A V}{\sigma_A} = \frac{R}{4L_A} \left( \frac{\sigma_A^*}{1 + M^* L^*} \right) \quad (5.2)$$

Where  $\sigma_A^* = 1 - \sigma_{AB}/\sigma_A - \sigma_B/\sigma_A$ ,  $M^* = \mu_B/\mu_A$  and  $L^* = L_B/L_A$ . This equation over predicts the values for the Ca number calculated using the data collected from this investigation. Another equation was developed from the same authors that includes the dissipation from the moving contact line. This new equation uses a  $V^*$  term to represent the maximum velocity of the bislug. The value for  $V^*$  could not be reproduced using the data from the paper.  $V^*$  may be an empirical fit for the data and would vary with channel geometry and fluid pairs.

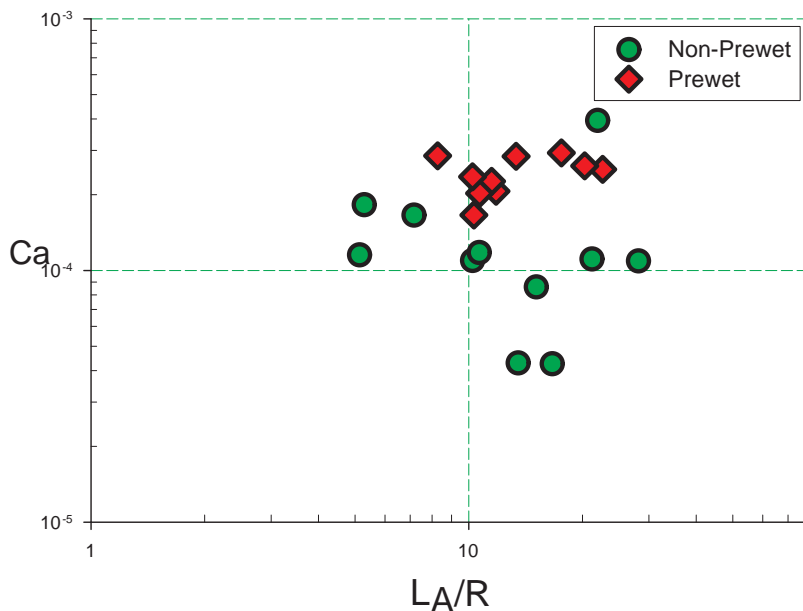


**Figure 5.1.** The prewet and non-prewet round data.

Bislug flow in round channels can be used to study the energy dissipation mechanism of slug flows. There are three primary dissipation mechanisms in slug flow; hydrodynamic interaction of proximate menisci, moving contact line, and wall shear stress. The wall shear stress was modeled based on Hagen-Poiseuille flow. As the slug grows in length, the wall drag will begin to dominate the dissipation mechanisms. The shear stress in the long slugs will dominate other dissipation mechanisms and this may provide a means of isolating this particular energy dissipation mechanism. A short slug is dominated by menisci interaction. As the slug shortens the recirculation present at each menisci will begin to interact with each other and dissipate energy. The final dissipation mechanism can be divided into two parts, the dragging of the contact line across the channel and the stretching of the interface at the menisci. Both of these dissipation mechanism are present at each menisci as the bislug flows down a microchannel.

The moving contact line dissipation is present in all slug flow, energy is lost as the menisci moves across the channel. As the slug moves down the channel, fluid is deposited from the menisci to the walls. This produces recirculation around the area where the meniscus contacts the wall reducing the energy in the system. As the front meniscus flows down the prewet microchannel the air-Fluid A thin film interface is destroyed. Energy is transferred from the stretched interface into the system as the front meniscus and thin film form a continuous interface. The amount of energy recovered is a function of the surface tension and the stretched area. The middle and rear menisci create new interfaces as the bislug travels down the channel. The middle meniscus produces the same thin film interface that is destroyed by the front

meniscus. In a single slug system the front and rear menisci have the same surface tension and the net energy exchange is zero but the difference in surface tension between the front and middle menisci in a bislug system produces a non-zero energy term. The rear menisci of Fluid B creates a thin over the existing thin film of Fluid A. This stretching term is normally neglected in single slug flows but it has a significant effect on the bislug system.

### 5.1.1 Comparison of Experimental Data & Model

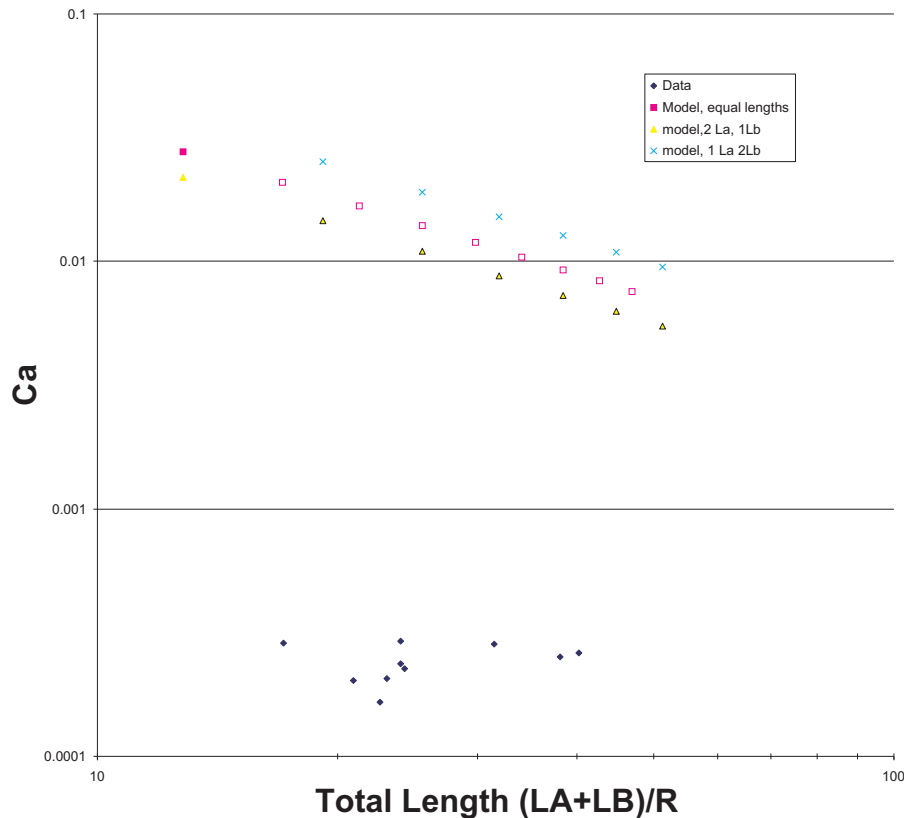


**Figure 5.2.** Ca numbers for both the model and the Prewet data, the model is based on equation ?? using a ratio of  $L_B/L_A = .5, 1, 2$

There is a magnitude or more difference in the values for the Ca numbers between the model and the data collected in the lab. Experimental data is plotted against the model in Figure 5.2, the plot uses values of 1/2, 1, and 2 for the ratio of the slug lengths. The differences between the model values and the actual Ca numbers can be attributed to the additional dissipation terms that are not present in the model. Menisci interactions begin to dominate the system as the slugs decrease in length and drag force decreases. Energy dissipation at the contact line is present in all slug flow and will produce an offset to the data set. As the slugs for both Fluid A and Fluid B increase in length the experimental data will approach the values predicted by the model. The model cannot predict the Ca number of short bislugs due to the



**Figure 5.3.** Bislug in a square channel.

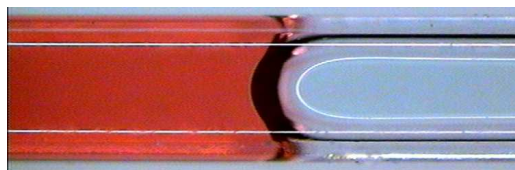


**Figure 5.4.** Fluid retention in the corner of a prewet square microchannel.

magnitude of the hydrodynamic interactions. A better understanding of this energy dissipation mechanism is needed; visualization data is needed near the menisci to accurately model this phenomenon.

## 5.2 Square Microchannels

Initially both dry and prewet cases were examined for bislug flow in square microchannels. Data from the dry microchannel test were found to be erratic. Since the microchannels satisfy the Concus-Finn criteria for corner flow, dry channels could not be maintained. When the ethylene glycol was introduced to the square microchannels, flow occurred spontaneously in the corners, the fluid retention in the corners can be seen on the right side of Figure 5.4. This, in effect, prewetted the corners and partially wetted the walls of microchannels. The partially prewet microchannels produced data having a large scatter which can be seen in Figure 5.5. It was later decided to focus the attention on prewet flow in square microchannels, which is the scenario that would be used in a micropump.

Velocities for bislug flow in square microchannels are presented in terms of velocity and Ca number, the velocities were non-dimensionalized using the same equation used for round tests, equation 5.1. Figures (5.7-5.8) have the Capillary numbers for the ethylene glycol as a function of the ethylene glycol and silicone oil slug lengths, the term  $L/R$  is a ratio of slug length to the radius of the channel,  $R=0.5\text{mm}$ .

Data is presented for the Capillary number for both the front and rear menisci, Figures (5.7-5.8). As the bislug moves, fluid is deposited on the walls of the channel and in the corners. Relative velocities for the front meniscus are slower than the velocities for the rear due to the volume of fluid being deposited. The coating thickness of the ethylene glycol has a maximum thickness in the corners and gradually decreases in thickness as it approaches the center of the sidewall. Using a darkfield lighting technique the amount of sidewall that is affected by the corner can be seen. The light was adjusted until the distance between the two dark bands remained constant, Figures 5.6(a-c). The volume of the fluid that is deposited can be determined by knowing the before and after lengths of the slug and the distance traveled. The film thickness can be estimated from the volume deposited and the length measured from darkfield images.

Bislug flow in square microchannels have a faster response time when compared with channels of circular cross-section, Figures 5.1, 5.7, and 5.8. The Capillary num-

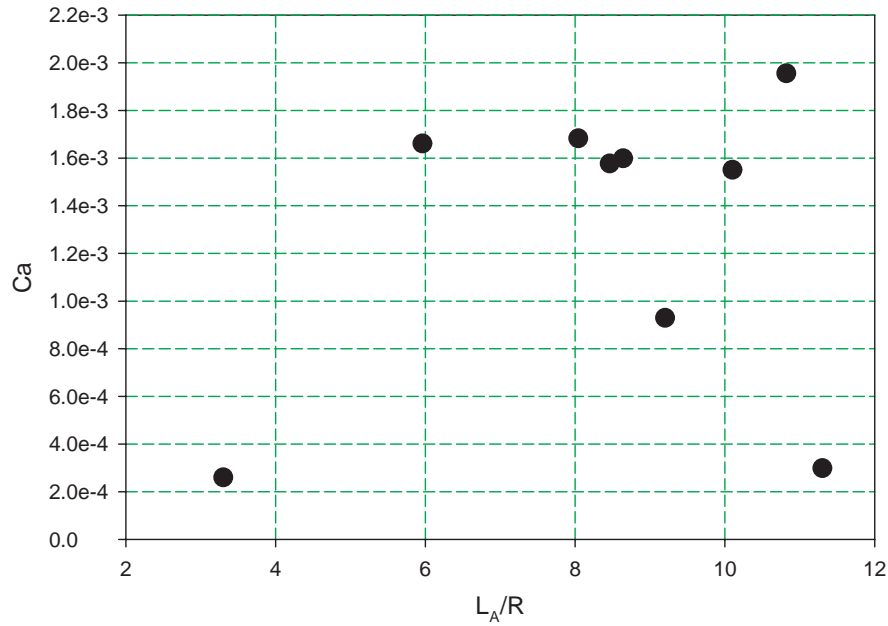


**Figure 5.5.** Graph of  $Ca$  for square dry channel

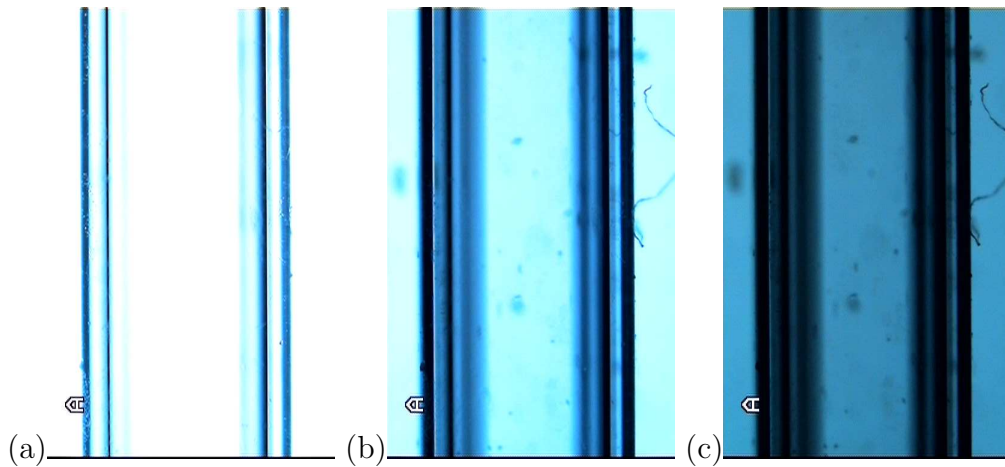


**Figure 5.6.** Images used to estimate the film thickness on the walls of a square microchannel. (a) Used for scaling images. (b) and (c) Used for measuring the amount of fluid retained in the corner and the width of the flat region of the prewet film.

ber in a prewet square microchannel is at least an order of magnitude greater than in round microchannels. Both systems have approximately the same pressure potential, the round was  $\Delta P=40.1$  Pa and the square  $\Delta=37.6$  Pa. The square channels have a hydraulic diameter of 1 mm, which results in a lower pressure because of the larger radius of curvature, and should exhibit a slower response, but the affects of the corners dominate the system (equation 4.10).

Fluid retention in the corners act like “rails” for the slugs to travel on. Energy dissipation associated with a moving contact line is reduced in this region from the increase in fluid thickness in and near the corners. Shear stress is also decreased in the system because the retained fluid reduces the effective area for the shear stress to act over. The losses associated with menisci interaction are still unknown and a reduction of energy dissipation in the this area cannot be determined.

The velocity of the bislug system has a dependency on the length of ethylene glycol while the length of silicone oil produces secondary effects. Figures 5.7 and 5.8 are the Ca numbers of the front and rear menisci as a function of slug lengths. From these figures, a correlation between slug length and speed can be seen for ethylene glycol. However, there is not a dependency between the silicone oil slug length and Ca number. This is due to the different fluid properties, the kinematic viscosity of the ethylene glycol is 16 times greater than that of the silicone oil. The viscous dissipation in the silicone oil slug is negligible compared to the ethylene glycol. The plots show the ratio between  $\mu_B$  and  $\sigma_B$  is small enough that the velocity term has little effect on the Capillary number for the silicone oil. The plots also show the same data that is presented in figures 5.7 and 5.8.

A model was developed to predict the response of a bislug in a square microchannel. An understanding of the energy dissipation in the system is needed to develop a working model. Moving contact line, menisci interaction, and shear stress at the wall are the primary forms of energy dissipation found in microchannel flow. Dissipation at the contact line is caused by the menisci being dragged across the channel wall. It has a constant affect on the system and is independent of slug length. As a slug gets longer shear stress becomes the dominant energy dissipation mechanism due to the increase in wall area. Short slugs, less than 3 diameters, have interactions between menisci. As the slug decreases in length the affect of of the shear stress decreases. Figures 5.9 and 5.10 show the three different regions of dissipation. Zone 1 is affected by contact line and menisci interations, Zone 2 is affected by all three dissipation mechanisms, and Zone 3 is affected by contact line and shear stress. It may be possible to study each of these mechanisms using bislug flow and a flow visualization technique, a force balance similar to the one developed for flow in a round channel will be developed.

Figure 5.11 compares the Capillary numbers from the experimental data to the Capillary numbers predicted from the developed model. Predictions from the two different models, without and with the stretching terms, were calculated using the low and high Capillary numbers from the data set. The models are dependent on the film thickness of A which is dependent on the Capillary number, this differs from the models for round channels where the thin film was assumed to be close to zero. The film in the corners, for fluid A, gets thicker due to the Concuss-Finn criteria and

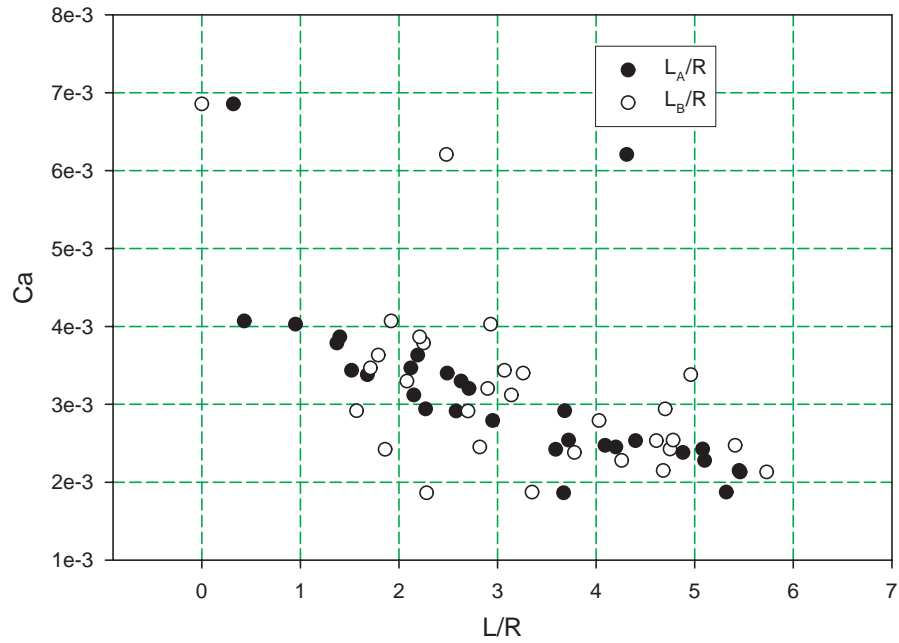


**Figure 5.7.** Ca number of ethylene glycol based on the front meniscus and the ratio of the slug length to the radius.

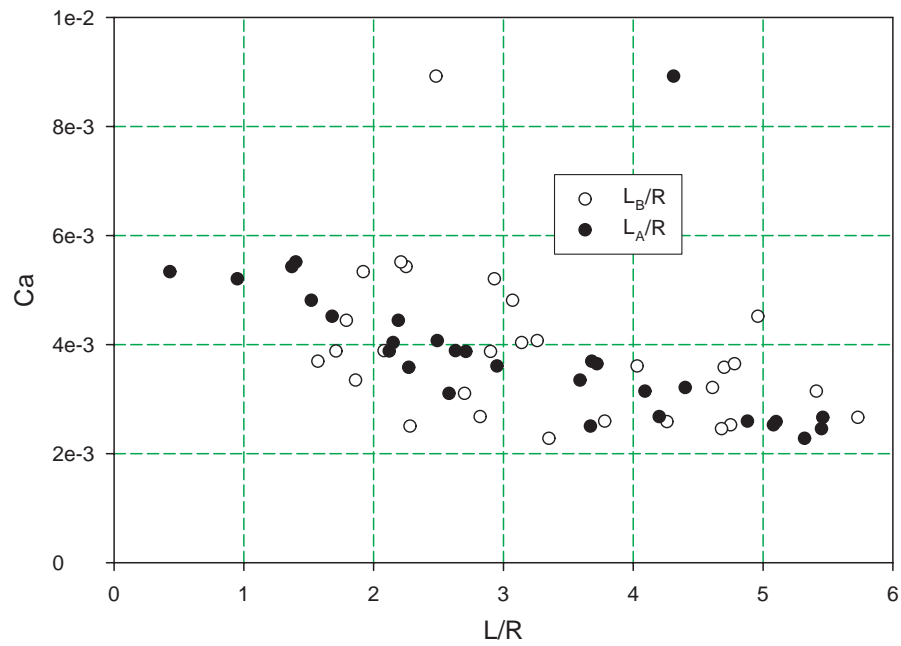


**Figure 5.8.** Ca number of ethylene glycol based on the rear meniscus and the ratio of the slug length to the radius.

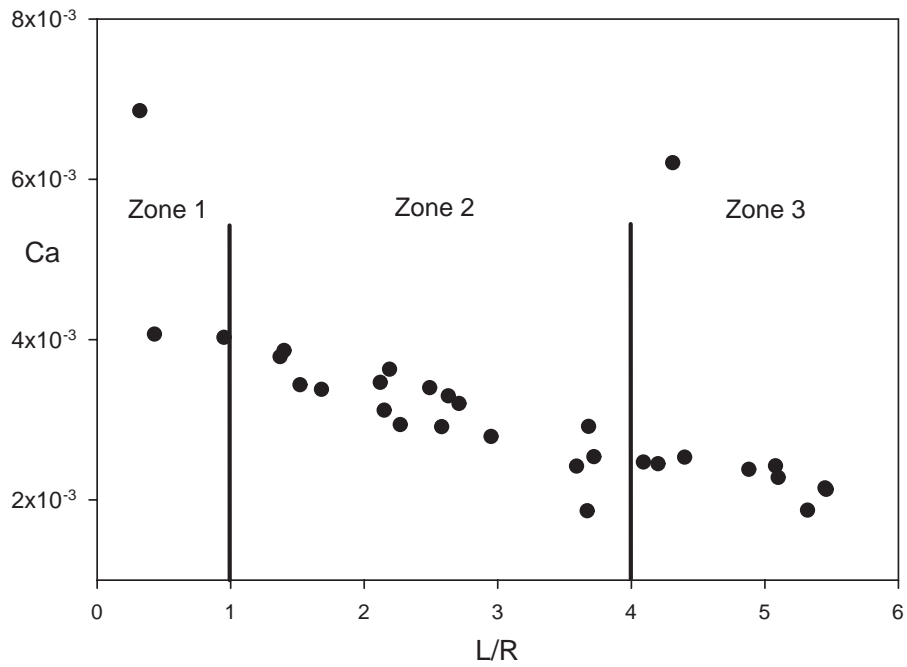


**Figure 5.9.** The different energy dissipation zones present in bislug system based on the data collected from the front meniscus.

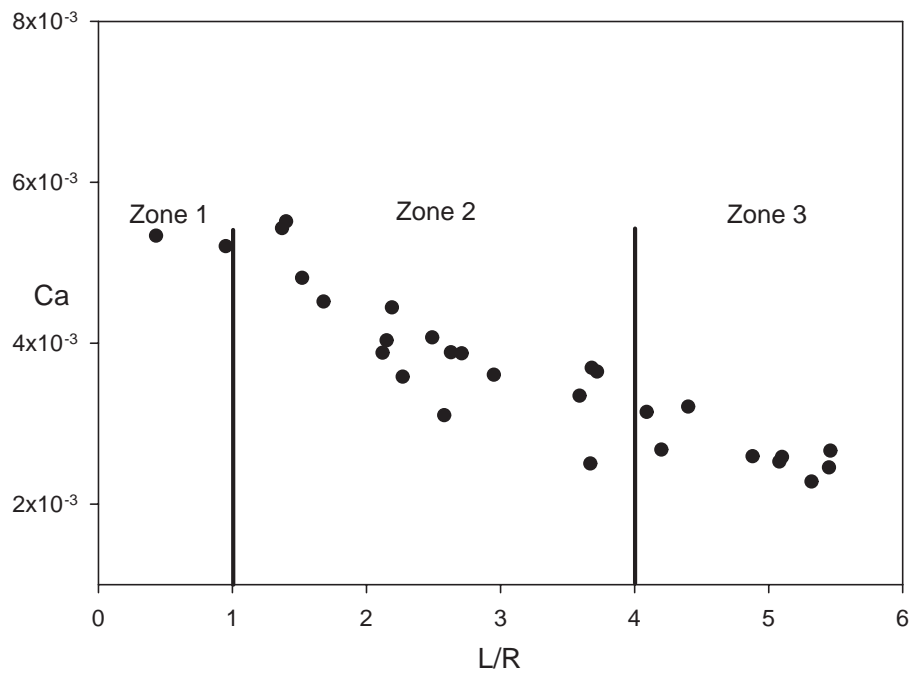


**Figure 5.10.** The different energy dissipation zones present in bislug system based on the data collected from the rear meniscus.

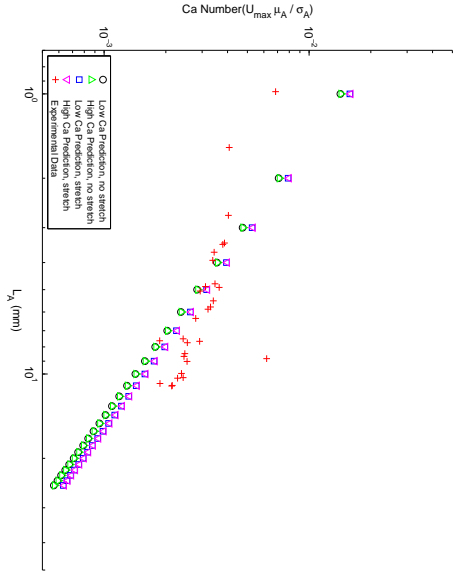


Figure 5.11.

can no longer be assumed to be small. The upper set of data,  $\nabla$  and  $\square$ , includes the interface stretching term, the lower set of data,  $\triangle$  and  $\circ$ , is the predictions without the interface stretching terms. As the slug decreases in length the role of the interface stretching increases, as the slugs get longer the predictions begin to collapse to a single line. This is expected as the drag will begin to dominate the system as the slug increases, the drag has a dependence on length.

For prewet square channels, fluid is retained in the corners of channel. This can be seen in Figure 5.4. A result of the spontaneous nature of the corner flow, the slug of ethylene glycol will begin to traverse the channel with the introduction of the second fluid. The slug will come to rest close to the middle of the channel when the pressure from the corners are balanced on both sides of the menisci. To produce a bislug the force of gravity is used to push the slug to one, silicone can be drawn into the glass through capillary forces. This may be a possible reason for the faster response in the microchannels and some inconsistencies in the data. A channel that was inverted longer during prewetting may produce a faster response than a channel that was inverted for a shorter period of time because of the amount of fluid that may have drained from the corners. When the tube is realigned horizontally, the pressure imbalance in the corners may help drive the flow for faster response.

B. G. Cox (1964). An experimental investigation of the streamlines in viscous fluid expelled from a tube. *Journal of Fluid Mechanics Digital Archive*, 20, pp 193-200 , hagen-poiseuille is valid upto 1.5 times the diameter to the menisci.

T.C. Thulasida, M.A. Abraham, R.L. Cerro, Dispersion during bubble-train flow in capillaries. *Chemical Engineering science*, 54, 1999, 61-76 Mention that when  $Ca < 10^{-4}$  corner flow from gravity is much larger than the flow in the film.

Could be a reason why data is inconsistent in some spots, too much drainage from the corners, results in a higher flow rate in the front meniscus, the length is much longer and the flowrate can increase.(check weislogel equation to verify). The length will decrease which will lesson the drag force but increase the hydrodynamic interactions.

## 6. FORCE TERMS

The derivation was performed using a force balance between the motive force the drag force and the interface stretching. There are other force terms that reduce the overall speed of the slug. These include the hydrodynamic interaction between menisci of short slugs and the energy dissipation at the contact line.

Dynamics of A liquid-liquid Interface in a capillary, Fermigier, M. , Jenffer, P., Ann Phys. ,13, 37-42 found that Cox(1986)'s empirical formula for dynamic contact angle for air-liquid displacement matched data when a fluid-fluid pair had a small viscosity ratio  $2/1$ , and some instances did not work at all. This Zhou and Sheng (1990) compare Fermigier and said true contact angle depends on contact line speed.

### 6.1 Hydrodynamic Interaction

Hydrodynamic interactions occur when a slug is small, less than two diameters. **need reference** A short slug has undeveloped streamlines and the menisci interfere with the velocity distribution. Slow moving slugs,  $Ca^{1/2} < .5$  produce vortices inside of the slugs. When two menisci are close the vortices interact with one another. This interaction shifts streamlines and dissipates energy in the form of viscous heating. **more** More understanding is needed to develop a model for the dissipation.

T.C. Thulasidas, M.A. Abraham and R.L Cerro, Flow patterns in liquid slugs during bubble train flow inside capillaries, Chemical Engineering Science, Vol 52, no 17, pp 2947-2962, 1997.

### 6.2 Contact Line

Energy dissipation associated with the moving contact line was not included in the force balance due to the complexity of the interactions at the interface. A problem that arises at the contact line is a singularity that is formed when assuming a no-slip boundary condition, the shear stress goes to infinity. Dussan(1976) removed the singularity by assuming a slip boundary condition, assuming the no-slip condition at the wall may no longer be valid. Ludviksson(1968) removed the singularity by assuming the channel was precoated by an advancing film ahead of the contact line. Using either assumption removes the physics from the local area and introduces new values that need numerical approximations or experimentally found values.

Contact line dissipation has been modelled using a dynamic contact angle approach. As a fluid moves across an interface, solid or fluid, the viscous stresses at the contact line distort the interface. This distortion changes the contact angles for the

system, the front increases and the rear decreases. In principle the local energy dissipation is captured by the dynamic contact angle,  $\theta_d$ . Cox(1986) provides a model for the dynamic contact angle for a liquid displacing a gas. Fermigier et al(1988) verified that the model could also be used for a liquid-liquid pair that had a small viscosity ratio. Van Der Zanden et al (1994) provides a model for moving liquid-liquid contact lines with small viscosity ratios. Their work is limited by a critical Ca number, a solution is not possible over this value. Though the physics at the contact line can be represented by the dynamic contact angle, it does not capture the true dissipation. The force balance for the bislug is *a priori* and does not include empirically found formulations.

Dynamics of A liquid-liquid Interface in a capillary, Fermigier, M. , Jenffer, P., Ann Phys. ,13, 37-42 1988

R. G. Cox (1986). The dynamics of the spreading of liquids on a solid surface. Part 1. Viscous flow. Journal of Fluid Mechanics Digital Archive, 168, pp 169-194

A. J. J. Van Der Zanden and A. K. Chesters, An approximate solution of the hydrodynamic problem associated with moving liquid-liquid contact lines. Int. J. Multiphase Flow, Vol 20, No 4., pp 789-798, 1994

E. B. Dussan V., The moving contact line: slip boundary condition, 1976, J. Fluid Mech, col 77, part 4, pp 665-684

Ludviksson, V. and Lightfoot, E. N, Deformation of advancing menisci, 1968 A.I.Ch.E J 14, 674

### 6.3 Non-Poiseuille flow

The flow profile for the slugs were assumed to be Classic Hagen-Poiseuille but there is evidence that the stream lines are not purely parabolic. Taylor(1961) presented sketches of possible streamlines in pressure driven bubble-train flow. When the  $Ca^{1/2} > .5$  the velocity streamlines bypass the bubble completely. If the  $Ca^{1/2} < .5$  recirculation vortices form in the slug. The velocity profiles are no longer classic Hagen-Poiseuille flow but are now treadlike. Prothero et al(1961) injected ink into slugs of liquid and noted that the ink travel the length of the slug after the slug had traveled two lengths. This was later verified by Thulasidas et al(1997) who noted the same time interval for a particle to travel one length of the slug. Also, micro-PIV images were included that proved the flow patterns predicted by Taylor(1961) were correct. The flow in a slug is not Poiseuille but treadlike. Dussan et al(1974) showed treadlike flows in a drop rolling along a solid. This same idea can be extrapolated to a drop in a microchannel with substrate on all sides.

The Ca numbers for these experiments result in a  $Ca^{1/2} < .5$ , this suggests that bislug flow has internal treadlike profiles. These internal circulations would destroy energy in the slugs through viscous heating(need reference to book). Bruno (?), using  $\mu$ PIV in square microchannels, reports the flow to be treadlike and not classic Hagen-Poiseuille flow as previously suggested, but the experimental results are preliminary. Further investigation is needed for development of a flow profile resembling those found in the slugs.

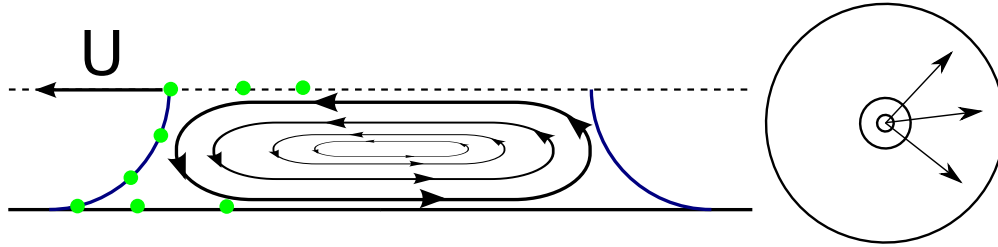


**Figure 6.1.** Recirculation caused by faster centerline velocity relative to the menisci, faster velocity is required to satisfy the conservation of mass for the system.

The treadlike flow profile may be the result of the conservation of mass in a 3-D configuration. The centerline velocity has to be faster than the menisci velocity to maintain the conservation of mass on the surface. As the green particles, from figure 6.1, are traced right to left the particles move from the center to the menisci and are lastly deposited on the wall. FINISH

G.I. Taylor, Deposition of a viscous fluid on the wall of a tube, 1961, *J. Fluid Mech.*, 10 pp 161-65

E.B. Dussan V. and S.H. Davis, The motion of a fluid-fluid interface, 1974, *J. Fluid Mech.* vol 65, part 1, pp71-95. Found a treadlike rolling of a drop on a solid substrate, can be similar to flow in channels.

T.C. Thulasidas, M.A. Abraham and R.L Cerro, Flow patterns in liquid slugs during bubble train flow inside capillaries, *Chemical Engineering Science*, Vol 52, no 17, pp 2947-2962, 1997.

Prothero and Burton 1961 *biophysics*, 1, 565-575. The physics of blood flow in capillaries-I the nature of motion.

## 6.4 Corner Flow

The velocity profile for the thin film in the square channels were assumed to be Couette or linear. Weislogel(1996) provides data and equations that quantify the amount of liquid being pumped into the corners from the meniscus. Pumping from the meniscus was verified by the use of a laser scanning confocal microscope at Sandia National Labs, Appendix A. Figure A.1 shows excited particles in a slug of ethylene glycol, as the slug remains stationary, fluid is pumped from the meniscus to the corner.

Couette flow was assumed for the film but a pumping force from the center meniscus in the opposite direction will produce a different profile in the film. For the leading meniscus, fluid is being pumped ahead of the meniscus as it travels down the channel. This may increase the velocity of the overall system. When the bislug was produced the channel was first dipped in ethylene glycol and inverted to coat the channel. The amount of time the channel was inverted may have added an uncertainty to the problem. The amount of fluid drained from the corners may have changed from test run to test run, see Chapter 5. This additional flowrate, along with the thicker film in the corners, may be the reason for the faster flows in microchannels that have corners and satisfy the Concus-Finn criteria.

## 7. CONCLUSION

Spontaneous bislug flow can occur in microchannels of circular and non-circular cross-sections. Microchannels with corners are subject to the Concus-Finn criteria. Fluid retention in the corners reduces the energy dissipation associated with the moving contact line and shear stress. The thicker fluid in the corners act like lubricating “rails” for the fluid to travel along.

A model has been developed that uses a balance of the pressure difference over of the menisci with the drag force and the force associated with the stretching of the interfaces at the menisci. Values for the experimental data are lower than those calculated using the model. The difference between the model and the data can be attributed to the energy dissipation mechanisms absent from the model; the additional mechanisms can be studied using this model and additional data. Bislug flow is a constant pressure system which will provide a repeatable test condition. The three major energy dissipation mechanisms can be studied using this technique. Short slugs will provide information on menisci interaction, long slugs will verify models for shear stress at the wall, and contact line dissipation can be studied from the transition from long to short slug lengths. The interface stretching term is important for shorter slugs.

A bislug in a square microchannel has a fast enough response time to be used for a micropump. To increase the response time a channel with corners should be used. The larger the corner angle the more fluid that can be retained which will decrease the amount of dissipation in the system. A micropump similar to the one in Figure ?? can be built using two immiscible fluids with known properties that are wetting to microchannel. The capillary pressures can be adjusted by changing the radius of curvature or surface tension. Adjusting the radius of curvature is preferred because of the limited number of working fluid pairs. The radius of curvature, in the viewing section, will be maintained provided the bislug spans the appropriate sections of the channel.

# APPENDIX

## A. CONFOCAL IMAGING OF CORNER FLOW

### A.1 *Sandia*

As previously discussed, the response time of the bislug is an important factor when designing a micropump. Microchannels of square cross-section produce a faster bislug flow than microchannels of round cross-section. To properly predict the response of the system, an understanding of the energy dissipation is needed. Visualization of the flow fields in a slug is hindered by the meniscus. The meniscus acts like a lens diverting light as it passes through. The menisci curvature prevents the viewing of the center line of the slug near the menisci. This region is of interest for studying dissipations caused by both the contact line and menisci interaction. To visualize flow in this area a confocal microscope may be used. A graduate student, J. Hernandez, was sent to Sandia National Laboratory in Albuquerque, New Mexico to determine whether a laser scanning confocal microscope (LSCM) could be used to study the flow patterns and the dissipation mechanism in bislug flow.

The LSCM uses a laser to excite a sheet of fluorescent particles. The light is collected through a pinhole that scans across a CCD sensor. The system at Sandia was capable of exciting and recording at two different light frequencies. Fluorescent coated polystyrene beads with a diameter of 15  $\mu\text{m}$  (Duke Scientific) and excitation frequencies of 468 nm and 542 nm, and emitting frequencies of 508 nm and 612 nm, were mixed in the ethylene glycol and silicone, respectively. Larger beads were used to decrease the system's dependency on lighting. As the beads decrease in diameter the amount of light emitted also decreases. Using larger beads avoided the potential problems associated with decreased light emittance. An ultrasonic water bath was used to break up the microbeads to produce a uniform dispersion; clumps of beads were still present after treatment and can be seen in Figure A.1. 100 cst silicone oil was used in place of the of 1 cst silicone oil to slow down the bislug, the LSCM has frame rate on the 0 of 1 fps which is too slow for the faster moving slugs.

Smaller square microchannels were used due to the optical limitations of the microscope. The depth of the 1 mm microchannels were outside the range of the microscope, so 500 and 300  $\mu\text{m}$  square channels were used. To control the slug lengths and trigger the flow, gates were made from Poly-DiMethyl Siloxane (PDMS). The primary design had a long central channel for the microchannel to fit into and two smaller channels branching off at the other end. Two syringes containing the working fluids were attached to the channels that branched off while a third needle, attached to a valve which opened to a syringe full of air or atmospheric pressure, was attached to the end of the long channel. The microchannel was prewet before being inserted into the PDMS. The branching channels were filled with fluid and the bislug was

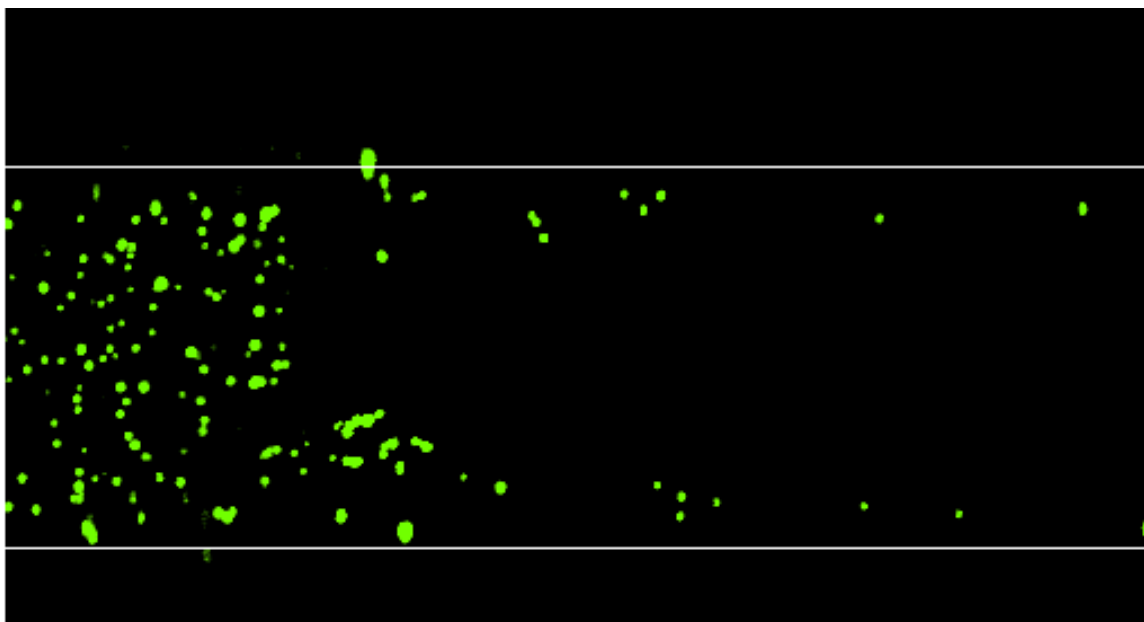


**Figure A.1.** Corner flow captured using a LSCM.

formed in the microchannel. The syringe full of air was used to break the bislug free and the system was then opened to atmospheric pressure. This method was only used a couple of times due to problems with the PDMS bonding. The dipping method, described earlier, was used instead.

Due to time constraints and system properties the data was recorded for visual purposes only, the slow frame rate and the linescanning image capture method produced images that were skewed. Images of the spontaneous flow in the corners were recorded. Figure A.1 shows a single frame. The flow was slower and could be accurately captured by the LSCM. Fluid flowed from the center of the meniscus to the corners. This may explain why the slug of ethylene glycol would traverse towards the middle of the channel. The slug would move as the fluid was being pulled from the center to the corners. Another issue with the LSCM is evident in Figure A.1 at the top of the channel. The gain for the camera had to be adjusted so beads were large enough to be seen but not too large that the beads appeared outside of the channel, which is what happened in this case. To prevent this a trial and error method was used to adjust the size of the beads for particle recording. A LSCM is capable of capturing the flow near a moving bislug meniscus but the slow frame rate produces images that are not quantifiable. The images captured were skewed and had too large of a distance traveled between particles for tracking accurately.

## B. ROUND DERIVATION

### B.1 Derivation of Force Terms

Three terms are included in the force balance; the motive force, the drag force and the force associated with the stretching of the interface at the menisci.

$$F_{\text{motive}} = F_{\text{drag}} + F_{\text{stretch}} \quad (\text{B.1})$$

#### B.1.1 Pressure Force

The motive force is caused by a pressure imbalance across the three menisci.

$$F_{\text{motive}} = \Delta P A_{\text{cross}} = \frac{2(\sigma_A - \sigma_B - \sigma_{AB})}{R} (\pi R^2) \quad (\text{B.2})$$

Where  $A_{\text{cross}}$  is the projected cross-sectional area of the menisci.

#### B.1.2 Interface Stretching

The stretching force was defined as the surface tension  $\sigma$  multiplied by the coated perimeter  $P_e$ . This occurs across each of three menisci in the bislug system.

$$F_{\text{stretch}} = \sigma P_e \quad (\text{B.3})$$

As the bislug flows in a prewet round channel there is a continuous destruction of the interface at A and the creation of one at AB and B. The creation at AB is done over the thin film  $h_A$ .

$$\begin{aligned} \text{Destruction of A-air interface} & : -\sigma_A 2\pi(R - h_A) \\ \text{Creation of A-B interface} & : \sigma_{AB} 2\pi(R - h_A) \\ \text{Creation of B-air interface} & : \sigma_B 2\pi(R - h_A - h_B) \end{aligned} \quad (\text{B.4})$$

$$\begin{aligned} F_{\text{stretch}} & = 2\pi R \left[ -\sigma_A \left(1 - \frac{h_A}{R}\right) + \sigma_{AB} \left(1 - \frac{h_A}{R}\right) + \sigma_B \left(1 - \frac{h_A}{R} - \frac{h_B}{R}\right) \right] \\ & = 2\pi R \left[ \left(1 - \frac{h_A}{R}\right) (\sigma_{AB} + \sigma_B - \sigma_A) - \sigma_B \frac{h_B}{R} \right] \end{aligned} \quad (\text{B.5})$$

### B.1.3 Drag Force

The drag force is divided into 3 terms, the core of slug A, the thin film of A beneath core B, and the core of B.

$$F = F_{\text{coreA}} + F_{\text{filmA}} + F_{\text{coreB}} \quad (\text{B.6})$$

#### Core A

Core A is modeled using the lubrication approximation.

$$0 = -\frac{\partial P}{\partial x} + \frac{\mu}{r} \frac{\partial}{\partial r} \left( r \frac{\partial u}{\partial r} \right) \quad (\text{B.7})$$

The pressure potential,  $\partial P/\partial x$ , is treated as a constant,  $K$ , which physically represents the pressure imbalance across the slug divided by the bislug length.

$$\frac{K}{\mu} = \frac{1}{r} \frac{\partial}{\partial r} \left( r \frac{\partial u}{\partial r} \right) \quad (\text{B.8})$$

Integrating twice to find the velocity and applying the no-slip condition at the wall and a symmetry condition at the centerline:

$$u = U_{\text{max}} \left[ 1 - \left( \frac{r}{R} \right)^2 \right] \quad (\text{B.9})$$

where

$$U_{\text{max}} = -\frac{KR^2}{4\mu} \quad (\text{B.10})$$

The shear stress at the wall is:

$$\tau_{wA} = \mu \frac{\partial u}{\partial r} \Big|_{r=R} = -\frac{2\mu AU}{R} \quad (\text{B.11})$$

#### Film A

Film A can be modeled as Couette flow. There is a no-slip condition on the wall and a moving boundary driven by Core B. Starting with lubrication approximation [B.7](#), with  $\partial P/\partial x$  being equal to zero and the  $\mu/r$  being constants, the working form becomes:

$$0 = \frac{\partial}{\partial r} \left( r \frac{\partial u}{\partial r} \right) \quad (\text{B.12})$$

Integrating twice

$$\begin{aligned} 0 &= \int \frac{\partial}{\partial r} \left( r \frac{\partial u}{\partial r} \right) \\ u &= C_0 \ln r + C_1 \end{aligned} \quad (\text{B.13})$$

Applying the boundary conditions:

$$\begin{aligned} \text{at } r = R, u &= 0 \\ \text{at } r = R - h_A, u &= U_{AB} \end{aligned} \tag{B.14}$$

Results in:

$$\begin{aligned} u &= C_0 \ln\left(\frac{r}{R}\right) \\ C_0 &= \frac{U_{AB}}{\ln(R - h_A)} \\ u &= U_{AB} \frac{\ln\left(\frac{R}{r}\right)}{\ln\left(\frac{R}{R - h_A}\right)} \end{aligned} \tag{B.15}$$

The final form [B.15](#) matches the previously derived solution for a set of concentric cylinders with the center cylinder in motion [??](#). The shear stress for the film can be found by taking the derivative of the velocity w.r.t the radius of the channel.

$$\tau = -\frac{\mu_A U_{AB}}{r \ln\left(\frac{R}{R - h_A}\right)} \tag{B.16}$$

Core B

Core B is modeled using the lubrication approximation in the same fashion as Core A [B.7](#).

$$u = \frac{K}{4\mu} r^2 + F(x) \ln(r) + g(x) \tag{B.17}$$

Applying the boundary condition at  $r = 0$

$$\begin{aligned} r &= 0, \text{ symmetry} \\ 0 &= \left. \frac{\partial u}{\partial r} \right|_{r=0} \\ &= \left. \frac{2Kr}{4\mu} + F'(x) \frac{1}{r} \right|_{r=0} \\ F'(x) &= 0 \rightarrow F(x) = 0 \\ u &= U_{max} \\ g(x) &= U_{max} \\ u &= \frac{k}{4\mu_B} r^2 + U_{max} \end{aligned} \tag{B.18}$$

Applying boundary condition at  $r = R - h_A$

$$\begin{aligned} u &= U_{AB}, \text{ at } r = R - h_A \\ U_{AB} &= \frac{k}{4\mu_B} (R - h_A)^2 + U_{max} \\ U_{max} &= U_{AB} - \frac{k}{4\mu_B} (R - h_A)^2 \end{aligned} \tag{B.19}$$

Solving for the velocity in terms of  $U_{AB}$ , combining equations B.18 and B.19:

$$\begin{aligned} u &= -\frac{k}{4\mu_B}(R-h_A)^2 \left(1 - \frac{r^2}{(R-h_A)^2}\right) \\ u &= (U_{max} - U_{AB}) \left(1 - \frac{r^2}{(R-h_A)^2}\right) + U_{AB} \end{aligned} \quad (\text{B.20})$$

The shear stress is:

$$\tau = -2\mu_B(U_{max} - U_{AB}) \frac{r}{(R-h_A)^2} \quad (\text{B.21})$$

#### B.1.4 Final Velocity Equations

$U_{AB}$  can be found from the boundary condition present at the film. The velocities and shear stresses are equal for both the film and the Core by assigning a zero slip boundary condition at a local point.

$$\begin{aligned} u_{filmA} &= u_{CoreB} = U_{AB} \\ \tau_{filmA}|_{r=R-h_A} &= \tau_{CoreB}|_{r=R-h_A} \end{aligned} \quad (\text{B.22})$$

This results in the solutions for film A at the boundary being:

$$\begin{aligned} u_{filmA} &= U_{AB} \\ \tau_{filmA} &= -\frac{\mu_A U_{AB}}{(R-h_A) \ln\left(\frac{R}{R-h_A}\right)} \end{aligned} \quad (\text{B.23})$$

Solutions for Core B are:

$$\begin{aligned} u_{CoreB} &= U_{AB} \\ \tau_{CoreB} &= -\frac{2\mu_B(U_{max} - U_{AB})}{R-h_A} \end{aligned} \quad (\text{B.24})$$

Setting equations B.23 and B.24 equal,  $U_{AB}$  can be solved.

$$U_{AB} = \frac{U_{max}}{1 + \frac{1}{2} \frac{\mu_A}{\mu_B} \frac{1}{\ln\left(\frac{R}{R-h_A}\right)}} \quad (\text{B.25})$$

The final form for the velocities and shear stress are:

$$\begin{aligned} u_{filmA} &= U_{max} \frac{\ln\left(\frac{R}{r}\right)}{\ln\left(\frac{R}{R-h_A}\right) + \frac{1}{2} \frac{\mu_A}{\mu_B}} \\ \tau_{filmA} &= -\frac{\mu_A U_{max}}{r \left(\ln\left(\frac{R}{R-h_A}\right) + \frac{1}{2} \frac{\mu_A}{\mu_B}\right)} \\ u_{CoreB} &= U_{max} \left(1 - \frac{1}{1 + \frac{1}{2} \frac{\mu_A}{\mu_B} \frac{1}{\ln\left(\frac{R}{R-h_A}\right)}}\right) \left(1 - \frac{r^2}{(R-h_A)^2}\right) \\ \tau_{CoreB} &= -2\mu_B U_{max} \frac{r}{(R-h_A)^2} \left(1 - \frac{1}{1 + \frac{1}{2} \frac{\mu_A}{\mu_B} \frac{1}{\ln\left(\frac{R}{R-h_A}\right)}}\right) \end{aligned} \quad (\text{B.26})$$

## Total Drag

When completing the final drag term,  $h_A$  and  $h_B$  are small and are ignored.

Fluid A:

$$\text{Core}(L_A) : \tau_w = -\frac{2\mu_A U_{max}}{R} \quad (\text{B.27})$$

$$\text{Film}(L_B) : \tau_w = -\frac{\mu_A U_{max}}{R \left( \ln \left( \frac{R}{R-h_A} \right) + \frac{1}{2} \frac{\mu_A}{\mu_B} \right)} \quad (\text{B.28})$$

Fluid B:

$$\text{Core}(L_{AB})\tau_w = -\frac{2\mu_B U_{max}}{R-h_A} \left( 1 - \frac{1}{1 + \frac{1}{2} \frac{\mu_A}{\mu_B} \frac{1}{\ln \left( \frac{R}{R-h_A} \right)}} \right) \quad (\text{B.29})$$

The total drag force is the sum of the drag forces from fluid A and fluid B.

$$\begin{aligned} F_{drag} &= \tau_{wA} A_{\text{Core}A} + \tau_{w\text{Film}A} A_{\text{Film}A} + \tau_{wB} A_{\text{Core}B} \quad (\text{B.30}) \\ &= \tau_{w\text{Film}}(2\pi R L_A) + \tau_{w\text{Film}}(2\pi R L_B) + \tau_{wB}(2\pi(R-h_A)L_B) \\ &= -\mu_A U_{max}(2\pi) \left( 2(L_A) + \frac{(L_B)}{\ln \left( \frac{R}{R-h_A} \right) + \frac{1}{2} \frac{\mu_A}{\mu_B}} + 2 \frac{\mu_B}{\mu_A} \left( 1 - \frac{1}{1 + \frac{1}{2} \frac{\mu_A}{\mu_B} \frac{1}{\ln \left( \frac{R}{R-h_A} \right)}} \right) (L_B) \right) \\ &= -\mu_A U_{max}(2\pi) \left( 2(L_A) + \frac{(L_B)}{\ln \left( \frac{1}{1-\delta} \right) + \frac{1}{2} \frac{\mu_A}{\mu_B}} + 2 \frac{\mu_B}{\mu_A} \left( 1 - \frac{1}{1 + \frac{1}{2} \frac{\mu_A}{\mu_B} \frac{1}{\ln \left( \frac{1}{1-\delta} \right)}} \right) (L_B) \right) \\ &= -\mu_A U_{max}(2\pi) \left( 2(L_A) + \frac{(L_B)}{\ln \left( \frac{1}{1-\delta} \right) + \frac{1}{2} \frac{\mu_A}{\mu_B}} + 2 \frac{\mu_B}{\mu_A} \left( 1 - \frac{\ln \left( \frac{1}{1-\delta} \right)}{\ln \left( \frac{1}{1-\delta} \right) + \frac{1}{2} \frac{\mu_A}{\mu_B}} \right) (L_B) \right) \\ &= -4\pi L_A \mu_A U_{max} \left( 1 + \frac{\mu_B L_B}{\mu_A L_A} + \frac{1}{2} \frac{L_B}{L_A} \frac{1}{\ln \left( \frac{1}{1-\delta} \right) + \frac{1}{2} \frac{\mu_A}{\mu_B}} - \frac{\mu_B L_B}{\mu_A L_A} \frac{\ln \left( \frac{1}{1-\delta} \right)}{\ln \left( \frac{1}{1-\delta} \right) + \frac{1}{2} \frac{\mu_A}{\mu_B}} \right) \\ &= -4\pi L_A \mu_A U_{max} \left( 1 + \frac{\mu_B L_B}{\mu_A L_A} + \frac{L_B}{L_A} \frac{1}{\ln \left( \frac{1}{1-\delta} \right) + \frac{1}{2} \frac{\mu_A}{\mu_B}} \left( \frac{1}{2} - \frac{\mu_B}{\mu_A} \ln \left( \frac{1}{1-\delta} \right) \right) \right) \quad (\text{B.31}) \end{aligned}$$

$\delta$  can be found by using the Bretherton relationship (?).

$$\delta = \frac{h_A}{R} = 1.34 \text{Ca}^{\frac{2}{3}} \quad (\text{B.32})$$

Assuming  $\delta$  is small because the Ca number is small. Therefore,  $\delta \ll 1$  and all the ln terms go to zero resulting in the final form of the drag.

$$F_{drag} = -4\pi L_A \mu_A U_{max} \left( 1 + 2 \frac{\mu_B L_B}{\mu_A L_A} \right) \quad (\text{B.33})$$

for  $\text{Ca} < 10^{-3}$ .

## B.1.5 Final Form

Finally the pressure force is set equal to the drag force and the stretching force.

$$\begin{aligned}
F_{\text{motive}} &= F_{\text{drag}} + F_{\text{stretch}} \\
\frac{2(\sigma_A - \sigma_B - \sigma_{AB})}{R} (\pi R^2) &= F_{\text{drag}} + \sigma_{AB} \left(1 - \frac{h_A}{R}\right) 2\pi R + \\
&\quad \sigma_B \left(1 - \frac{h_A + h_B}{R}\right) 2\pi R - \sigma_A \left(1 - \frac{h_A}{R}\right) 2\pi R \\
(\sigma_A - \sigma_B - \sigma_{AB}) &= \frac{F_{\text{drag}}}{2\pi R} + (\sigma_B + \sigma_{AB} - \sigma_A) \left(1 - \frac{h_A}{R}\right) - \sigma_B \frac{h_B}{R} \\
\left(1 - \frac{\sigma_B}{\sigma_A} - \frac{\sigma_{AB}}{\sigma_A}\right) &= \frac{F_{\text{drag}}}{2\pi R \sigma_A} + \left(\frac{\sigma_B}{\sigma_A} + \frac{\sigma_{AB}}{\sigma_A} - 1\right) \left(1 - \frac{h_A}{R}\right) - \frac{\sigma_B}{\sigma_A} \frac{h_B}{R} \\
\frac{F_{\text{drag}}}{2\pi R \sigma_A} &= \left(1 - \frac{\sigma_B}{\sigma_A} - \frac{\sigma_{AB}}{\sigma_A}\right) + \left(1 - \frac{\sigma_B}{\sigma_A} - \frac{\sigma_{AB}}{\sigma_A}\right) \left(1 - \frac{h_A}{R}\right) + \frac{\sigma_B}{\sigma_A} \frac{h_B}{R} \\
\frac{F_{\text{drag}}}{2\pi R \sigma_A} &= \left(1 - \frac{\sigma_B + \sigma_{AB}}{\sigma_A}\right) \left[1 + \left(1 - \frac{h_A}{R}\right)\right] + \frac{\sigma_B}{\sigma_A} \frac{h_B}{R} \\
\frac{F_{\text{drag}}}{2\pi R \sigma_A} &= \left(1 - \frac{\sigma_B + \sigma_{AB}}{\sigma_A}\right) \left(2 - \frac{h_A}{R}\right) + \frac{\sigma_B}{\sigma_A} \frac{h_B}{R} \tag{B.34}
\end{aligned}$$

Assume, as previously, that the ratio of film thickness to radius is small,  $h_B/R$ ,  $h_A/R \ll 1$ .

$$\begin{aligned}
\frac{F_{\text{drag}}}{2\pi R \sigma_A} &\approx 2 \left(1 - \frac{\sigma_B + \sigma_{AB}}{\sigma_A}\right) \\
\frac{F_{\text{drag}}}{4\pi R \sigma_A} &\approx \left(1 - \frac{\sigma_B + \sigma_{AB}}{\sigma_A}\right) \\
\frac{4\pi L_A \mu_A U_{\text{max}} \left(1 + 2 \frac{\mu_B}{\mu_A} \frac{L_B}{L_A}\right)}{4\pi R \sigma_A} &\approx \left(1 - \frac{\sigma_B + \sigma_{AB}}{\sigma_A}\right) \\
\frac{\mu_A U_{\text{max}} \left(1 + 2 \frac{\mu_B}{\mu_A} \frac{L_B}{L_A}\right)}{\sigma_A} &\approx \left(1 - \frac{\sigma_B + \sigma_{AB}}{\sigma_A}\right) \frac{R}{L_A} \tag{B.35}
\end{aligned}$$

The final form of the model is equation B.36.

$$Ca_{\text{max}} \approx \left[1 - \left(\frac{\sigma_{AB} + \sigma_B}{\sigma_A}\right)\right] \left(\frac{R}{L_A}\right) \left(\frac{1}{1 + 2 \frac{\mu_B}{\mu_A} \frac{L_B}{L_A}}\right) \tag{B.36}$$

for  $Ca < 10^{-3}$ .

The final form without the removal of the films: **SYMPLYFY**

$$Ca_{\text{max}} = \frac{1}{2} \frac{\left[\frac{\Delta\sigma}{\sigma_A}(2 - H_A) + \frac{\sigma_B}{\sigma_A} H_B\right]}{\left\{1 + \frac{L_B}{L_A} \left(\frac{\mu_B}{\mu_A} - \frac{L_B}{L_A} \frac{\frac{1}{2} + \frac{\mu_B}{\mu_A} \ln\left(\frac{1}{1-H_A}\right)}{\ln\left(\frac{1}{1-H_A}\right) + \frac{1}{2} \frac{\mu_A}{\mu_B}}\right)\right\}} \tag{B.37}$$

## C. SQUARE DERIVATION

### C.1 Derivation of Force Terms

Three terms are included in the force balance; the motive force, the drag force and the force associated with the stretching of the interface at the menisci, these are the same force terms used in the round derivation [B.1](#).

$$F_{\text{motive}} = F_{\text{drag}} + F_{\text{stretch}} \quad (\text{C.1})$$

#### C.1.1 Pressure Force

The motive force is caused by a pressure imbalance across the three menisci, a spherical cap is used for the shape of the square menisci, this results in the same pressure differential found for the round geometries.

$$F_{\text{motive}} = \Delta P A_{\text{cross}} = \frac{2(\sigma_A - \sigma_B - \sigma_{AB})}{R} (\pi R^2) \quad (\text{C.2})$$

Where  $A_{\text{cross}}$  is the projected cross-sectional area of the menisci.

The stretching force was defined as the surface tension  $\sigma$  multiplied by the coated perimeter  $P_e$ . This occurs across each of three menisci in the bislug system. To find the perimeter for a square channel with a film, the film was broken in to two parts, the flat film and the corner region [4.6](#). The transition begins where the radius of the corner has a perpendicular intersection with the wall. The shape of the corner is assumed to be a partial circle (1/8) with a radius  $R_c$ . For the leading slug the perimeter is that of a normal square.

$$F_{\text{stretch}} = \sigma P_e \quad (\text{C.3})$$

As the bislug flows in a prewet round channel there is a continuous destruction of the interface at A and the creation of one at AB and B. The creation at AB is done over the thin film  $h_A$ .

$$x_c = R - x_f = R_c + h_A \quad (\text{C.4})$$

Destruction of A-air interface :  $-\sigma_A 2\pi(R - h_A)$  **what should the perimeter be for the lead**

Creation of A-B interface :  $\sigma_{AB} 8R \left[ \frac{x_f}{R} + \frac{\pi}{4} \left( 1 - \frac{x_f}{R} - \frac{h_A}{R} \right) \right]$

Creation of B-air interface :  $\sigma_B 8R \left[ \frac{x_f}{R} + \frac{\pi}{4} \left( 1 - \frac{x_f}{R} - \frac{h_A}{R} - \frac{h_B}{R} \right) \right]$

$$\begin{aligned}
F_{\text{stretch}} &= 2\pi R \left(1 - \frac{h_A}{R}\right) (\sigma_{AB} + \sigma_B - \sigma_A) + 8x_f(\sigma_{AB} + \sigma_B) - 2\pi x_f(\sigma_{AB} + \sigma_B) - \sigma_B R \pi h_B \\
&= 2\pi R \left[ \left(1 - \frac{h_A}{R}\right) (\sigma_{AB} + \sigma_B - \sigma_A) - \frac{x_f}{R} (\sigma_{AB} + \sigma_B) - \sigma_B \frac{h_B}{R} \right] + 8x_f(\sigma_{AB} + \sigma_B)
\end{aligned} \tag{6}$$

### C.1.2 Geometry

To keep a similar derivation with the round channels a distance from the center of the square channel was used. This is broken into two different sections, geometry for the flat region and corner region.

#### Flat Region

The distance to the film:

$$\begin{aligned}
S_f &= \sqrt{x^2 + (R - h_A)^2} \\
\sigma_f = \frac{S_f}{R} &= \sqrt{\zeta^2 + (1 - H_o)^2}
\end{aligned} \tag{C.7}$$

Where  $\zeta$  is the ratio  $x/R$  and  $H_o$  is  $h_A/R$ .

The distance to the wall:

$$\begin{aligned}
S_o &= \sqrt{x^2 + R^2} \\
\sigma_o = \frac{S_o}{R} &= \sqrt{\zeta^2 + 1^2}
\end{aligned} \tag{C.8}$$

#### Corner Region

The distance from the center to the wall is the same for the corner and flat region.

$$\begin{aligned}
h_c &= \sqrt{(x - x_f)^2 + (R_c + h_A)^2} - R_c \\
h_c' &= \frac{R_c + h_o}{R_c + h_c} h_c \\
x^* &= x - h_c \frac{x - x_f}{R_c + h_c} \\
S_f &= \sqrt{x^{*2} + (R - h_c')^2}
\end{aligned} \tag{C.9}$$

Non-dimensionalized

$$\begin{aligned}
H_c = \frac{h_c}{R} &= \sqrt{(\zeta - \zeta_f)^2 + (C + H_o)^2} - C \\
H_c' = \frac{h_c'}{R} &= H_c \frac{C + H_p}{C + H_c} \\
\zeta_x = \frac{x^*}{R} &= \zeta - H_c \frac{\zeta - \zeta_f}{C + H_c} \\
\sigma_f = \frac{S_f}{R} &= \sqrt{\zeta_x^2 + (1 - H_c')^2}
\end{aligned} \tag{C.10}$$

## C.2 Drag

### C.2.1 Velocity Derivations

#### Core A

Assuming Poiseuille flow in the channel and using  $S$  as a distance function, this allows for the same derivation technique used in the round channels. The distance from the center to the wall and the film increases as  $z$  increase from the center to the wall.

starting with the lubrication approximation,  $s$  can be substituted for  $R$ , both distance measurements from the center point of the channel.

$$0 = -\frac{\partial P}{\partial z} + \frac{\mu}{s} \frac{\partial}{\partial s} \left( s \frac{\partial u}{\partial s} \right) \quad (\text{C.11})$$

Integrating twice w.r.t  $s$ ,

$$u = \frac{1}{2} C_0 s^2 + C_1 s + c_2 \quad (\text{C.12})$$

Boundary conditions:

$$\begin{aligned} u = U_{max} \quad @ \quad s = 0 &\rightarrow U_{max} = C_2 \\ \frac{\partial u}{\partial s} = 0 \quad @ \quad s = 0 &\rightarrow C_1 = 0 \\ u = 0 \quad @ \quad s = S_o &\rightarrow C_0 = \frac{-2U}{U_{max}} \end{aligned} \quad (\text{C.13})$$

Results in:

$$u = U_{max} \left[ 1 - \frac{s^2}{S_o^2} \right] \quad (\text{C.14})$$

a generic solution for Poiseuille.

Shear Stress at the wall:

$$\tau_w = \mu_A \frac{\partial u}{\partial s} \Big|_{s=S_o} = \mu_A \frac{2U_{max}}{S_o} \quad (\text{C.15})$$

#### Film A

Starting with the lubrication approximation, same as derivation for round channels

$$0 = \frac{\partial}{\partial s} \left( s \frac{\partial u}{\partial s} \right) \quad (\text{C.16})$$

Integrating twice

$$\begin{aligned} 0 &= \int \frac{\partial}{\partial r} \left( r \frac{\partial u}{\partial r} \right) \\ u &= C_0 \ln s + C_1 \end{aligned} \quad (\text{C.17})$$

$$\begin{aligned}
u = 0 & \quad @s = S_o \quad \rightarrow C_1 = -C_0 \ln S_o \\
u = U_{AB} & \quad @s = S_f \quad \rightarrow C_0 = \frac{U_{AB}}{\ln \frac{S_f}{S_o}}
\end{aligned} \tag{C.18}$$

results in:

$$\begin{aligned}
u &= C_0 \ln \frac{s}{S_o} \\
C_o &= \frac{U_{AB}}{\ln \frac{S_f}{S_o}} \\
u &= U_{AB} \frac{\ln \left( \frac{s}{S_o} \right)}{\ln \left( \frac{S_f}{S_o} \right)} \\
\text{or, } u &= U_{AB} \frac{\ln \left( \frac{S_o}{s} \right)}{\ln \left( \frac{S_o}{S_f} \right)}, \text{ to match the solution for a round channel} \tag{C.19}
\end{aligned}$$

### Core B

Starting with the lubrication approximation, same as Core A.

$$0 = -\frac{\partial P}{\partial z} + \frac{\mu}{s} \frac{\partial}{\partial s} \left( s \frac{\partial u}{\partial s} \right) \tag{C.20}$$

Integrating twice w.r.t s,

$$u = \frac{k}{4\mu_A} s^2 + C_1 s + C_2 \tag{C.21}$$

$$k = \frac{\partial P}{\partial z}$$

Boundary conditions:

$$\begin{aligned}
u = U_{max} & \quad @ s = 0 \quad \rightarrow U_{max} = C_2 \\
\frac{\partial u}{\partial s} = 0 & \quad @ s = 0 \quad \rightarrow C_1 = 0 \\
u = U_{AB} & \quad @ s = S_f \quad \rightarrow U_{AB} = \frac{k}{4\mu_A} S_f^2 + U_{max}
\end{aligned} \tag{C.22}$$

$$\tag{C.23}$$

The velocity is:

$$u = \frac{k}{4\mu_A} s^2 + U_{max} \tag{C.24}$$

### Final Velocity Forms

$U_{AB}$  can be found in the same fashion as the round channels. At the transition between film A and Core B it is assumed to have a no-slip condition. This results in a constant velocity and shear stress at a local point at the transition.

B.C.'s

$$\begin{aligned} \tau_{coreB}|_{s=S_f} &= \tau_{filmA}|_{s=S_f} \\ u_{coreB}|_{s=S_f} &= u_{filmA}|_{s=S_f} = U_{AB} \end{aligned} \quad (C.25)$$

(C.26)

$$\begin{aligned} \tau_{coreB}|_{s=S_f} &= \mu_B \frac{\partial u}{\partial s}|_{s=S_f} = -\mu_B (U_{max} - U_{AB}) \frac{2}{S_f} \\ \tau_{filmA}|_{s=S_f} &= \mu_A \frac{\partial u}{\partial s}|_{s=S_f} = -\mu_A \frac{U_{AB}}{S_f \ln \frac{S_o}{S_f}} \end{aligned} \quad (C.27)$$

Combining the shear stress and velocities at the transition results in:

$$U_{AB} = \frac{U_{max}}{\left(1 + \frac{1}{2} \frac{\mu_A}{\mu_B} \frac{1}{\ln \frac{S_o}{S_f}}\right)} \quad (C.28)$$

non-dimensional:

$$\frac{U_{AB}}{U_{max}} = \frac{1}{\left(1 + \frac{1}{2} \frac{\mu_A}{\mu_B} \frac{1}{\ln \frac{\sigma_o}{\sigma_f}}\right)} \quad (C.29)$$

Resulting Final Equations:

$$u_{filmA} = U_{max} \frac{\ln \frac{s}{S_o}}{\ln \frac{S_o}{S_f} + \frac{1}{2} \frac{\mu_A}{\mu_B}} \quad (C.30)$$

$$u_{CoreB} = U_{max} \left[ \left(1 - \frac{s^2}{S_f^2}\right) + \frac{\frac{s^2}{S_f^2}}{\left(1 + \frac{1}{2} \frac{\mu_A}{\mu_B} \frac{1}{\ln \frac{S_o}{S_f}}\right)} \right] \quad (C.31)$$

Both equations are a function of x, resulting in different profiles at different locations of x. Each of the functions for s have been described in the geometry section. The functions must be used in the correct location in the channel. or, non-dimensionalized

$$Ca_A = Ca_{Amax} \left[ \left(1 - \frac{\sigma^2}{\sigma_f^2}\right) + \frac{\frac{\sigma^2}{\sigma_f^2}}{\left(1 + \frac{1}{2} \frac{\mu_A}{\mu_B} \frac{1}{\ln \frac{\sigma_o}{\sigma_f}}\right)} \right] \quad (C.32)$$

where,

$$Ca_A = U_{max} \mu_A / \sigma_A \quad (C.33)$$

## C.2.2 Final Forms of Drag

Drag force is the shear stress acting over the surface area.

Shear stresses,

$$\begin{aligned}\tau_{wCoreA} &= -2\mu_A \frac{U_{max}}{S_o} \\ \tau_{wFilmA} &= -\mu_A \frac{U_{AB}}{S_o \ln\left(\frac{S_o}{S_f}\right)} \\ \tau_{fCoreB} &= -2\mu_B \frac{(U_{max} - U_{AB})}{S_f}\end{aligned}\tag{C.34}$$

where,

$$U_{AB} = \frac{U_{max}}{\left(1 + \frac{1}{2}M \frac{1}{\ln\left(\frac{S_o}{S_f}\right)}\right)}\tag{C.35}$$

where,  $M = \frac{\mu_A}{\mu_B}$ .  
non-dimensionalized distance,

$$\begin{aligned}\tau_{wCoreA} &= -2\mu_A \frac{U_{max}}{\sigma_o} \\ \tau_{wFilmA} &= -\mu_A \frac{U_{AB}}{\sigma_o \ln\left(\frac{\sigma_o}{\sigma_f}\right) R} \\ \tau_{fCoreB} &= -2\mu_B \frac{(U_{max} - U_{AB})}{\sigma_f R}\end{aligned}\tag{C.36}$$

Where,

$$U_{AB} = \frac{U_{max}}{\left(1 + \frac{1}{2}M \frac{1}{\ln\left(\frac{\sigma_o}{\sigma_f}\right)}\right)}\tag{C.37}$$

where,  $M = \frac{\mu_A}{\mu_B}$ .

Core A

$$\begin{aligned}F_{dragCoreA} &= \int \int \tau_{wCoreA} \partial x \partial z \\ &= l_A \int \tau_{wCoreA} \partial x\end{aligned}\tag{C.38}$$

A closed form solution exists for the leading slug, Core A.

$$F_{dragcoreA} = -16l_A U_{max} \mu_A \ln(1 + \sqrt{2})\tag{C.39}$$

### Film A and Core B

Film A and Core B must be numerically integrated to find the values for the drag. The viscosity ratio must be included in the integration making each solution unique to the fluid pairs.

Core B:

$$\begin{aligned} F_{dragCoreB} &= \int \int \tau_{fCoreB} \partial x \partial z \\ &= l_b \int \tau_{fCoreB} \partial x \end{aligned} \tag{C.40}$$

Film A:

$$\begin{aligned} F_{dragFilmA} &= \int \int \tau_{wFilmA} \partial x \partial z \\ &= l_b \int \tau_{wFilmA} \partial x \end{aligned} \tag{C.41}$$

The numerical integration has to take place over different domains. The domains are the flat region and the corner. The interface that the shear stress acts over needs to be integrated over the distance normal to the surface. The distance equations can be found above [C.1.2](#).

The non-dimensional form was used so the integration was from 0-1 for Core A and from 0- $\zeta_{trans}$  for the flat region and  $\zeta_{trans}-1$  for the corner region. The substitution of the distance equations and  $U_{AB}$  result in equations that cannot be solved analytically but require numerical integration.

Coefficients were used for the solution of the drag forces, the drag from Core B and Film A were combined and  $\alpha$  was used for the coefficient. Core A has a closed form solution but  $\beta$  was used for the coefficient for consistency.

$$\begin{aligned} F_{dragCoreA} &= \beta U_{max} L_A \\ F_{dragCoreB} + F_{dragFilmA} &= \alpha U_{max} L_B \end{aligned} \tag{C.42}$$

### C.3 Force Balance

Setting the motive force equal to the drag and stretching.

$$F_{motive} = F_{drag} + F_{stretch} \tag{C.43}$$

$$\begin{aligned} &\frac{2(\sigma_A - \sigma_B - \sigma_{AB})}{R} (2\pi R^2) \frac{\pi}{4} R^2 = \\ &\alpha U_{max} L_B + \beta U_{max} L_A \mu_A \\ &+ 2\pi R \sigma_A \left[ \left(1 - \frac{h_A}{R}\right) \left(\frac{\sigma_{AB} + \sigma_B}{\sigma_A}\right) - \frac{x_f}{R} \left(1 - \frac{4}{\pi}\right) \left(\frac{\sigma_{AB} + \sigma_B}{\sigma_A}\right) + \frac{h_B}{R} \frac{\sigma_B}{\sigma_A} \right] \end{aligned}$$

$$U_{max} L_A \mu_A \left( \frac{\alpha L_B}{\mu_A L_A} + \beta \right) = \quad (C.44)$$

$$2\pi R \sigma_A \left[ \left( \frac{\sigma_{AB} + \sigma_B}{\sigma_A} \right) \left( 2 - \frac{h_A}{R} \right) + \frac{x_f}{R} \left( 1 - \frac{4}{\pi} \right) \left( \frac{\sigma_{AB} + \sigma_B}{\sigma_A} \right) \right] \quad (C.45)$$

The final form has been non-dimensionalized using  $Ca_A$ , assumes  $h_B \ll 1$  to simplify the equation and the film thickness is found by using the Bretherton relationship.

$$Ca_{Amax} = \frac{U_{max} \mu_A}{\sigma_A} = \frac{2\pi R \left[ \left( \frac{\sigma_{AB} + \sigma_B}{\sigma_A} \right) \left( 2 - \frac{h_A}{R} \right) + \frac{x_f}{R} \left( 1 - \frac{4}{\pi} \right) \left( \frac{\sigma_{AB} + \sigma_B}{\sigma_A} \right) \right]}{L_A \left( \frac{\alpha L_B}{\mu_A L_A} + \beta \right)} \quad (C.46)$$

**Table C.1.** Coefficients for  $F_{drag}$  in the square channels

Ca Number	$h_o$ ( $\mu\text{m}$ )	$\alpha$ (kg/m s)	$\beta$
2 E-3	10.6	0.52567	14.1020
4 E-3	16.9	0.51926	14.1020

Without Stretch term:

$$Ca_{Amax} = \frac{2\pi R}{L_A} \frac{1 - \left( \frac{\sigma_{AB} + \sigma_B}{\sigma_A} \right)}{\frac{\alpha L_B}{\mu_A L_A} + \beta} \quad (C.47)$$

need to finish the derivation after matlab code is finished up.

## D. MATLAB CODE

### D.1 graphing

*Modeling the velocity profiles in both round and square channels with and without a thin film*

*Stepping Through Velocities,*

```
n=.00005;    % step size

Ca_r=[4E-5 2E-4 2E-4 3E-4];           % Data from
    experiments
Ca_label_r=cellstr(['Round_Non-Prewet_low_'; 'Round_Non-
    Prewet_high'; 'Round_Prewet_low_'; 'Round_Prewet_high_'])
    ;           %labels for the data

sigma_A=47.7e-3 ;           %N/m
mu_A=.0178;           % kg/(m s)
Umax_r=Ca_r*sigma_A/mu_A*1000 ;           %
    mm/s

%Umax=200;           % mm/s

R=.5;           % half width of the channel for the square
    and the radius for the round

ho_r=R*.643*(3.*Ca_r).^(2/3);           % mm, calculated
    from bretherton1961

%ho=[.01 .05 .1];

    Outer Loop, Stepping Through ho

for i=1:length(ho_r);
```

*Round Channels*

Properties For a bislug system the front and film are function of fluid A and the rear is a function of fluid B

---

```

zeta_coreA=0:n:1;    % non dimensionalized position in r  zeta=r/
                    R

%ho=.1;
H(i)=ho_r(i)/R;    % non dimensionalized film thickness H=
                  ho/R

muA=.0178;    % kg/(m s)
muB=.0096;    % kg/(m s);

zeta_Film_boundary(i)=1-H(i);

for j=1:length(zeta_Film_boundary(i):n:1);    % calculating
    zeta for film A
    a=zeta_Film_boundary(i):n:1;
    zeta_FilmA(i,j)=a(j);

end
clear a

for j=1:length(0:n:zeta_Film_boundary(i));    %
    calculating zeta for core B
    a=0:n:zeta_Film_boundary(i);
    zeta_CoreB(i,j)=a(j);
end
clear a

                    Poiseuille flow (ur=Umax(1-zeta^2))

for j=1:length(zeta_coreA)
ur_CoreA(i,j)=Umax_r(i)*(1-zeta_coreA(j).^2); % ur_A is the flow
    in the round channel w.r.t. fluid A
end    % doesn't need loop,
    only one series of values because it is in Core A

                    Velocity of film

UABr(i)=Umax_r(i)./(1-1/2*muA/muB.*1./log(1-H(i)));

                    Poiseuille with film

for j=1:length(zeta_CoreB(i,:))
ur_CoreB(i,j)=Umax_r(i)*((1+zeta_CoreB(i,j))^2/(1-H(i))^2*(1/(1-
    muA/(2*muB)*1/log(1-H(i))-1)));
end

```

*Couette Flow in thin film*

```

for j=1:length(zeta_FilmA(i,:))
ur_FilmA(i,j)=Umax_r(i)*log(zeta_FilmA(i,j))/(log(1-H(i))-1/2*muA
    /muB);
end

end

```

*Plots of Round channels*

```

for i=1:length(ho_r);
% round w/o film

figure
hold on
% Core A
plot(ur_CoreA(i,:)/Umax_r(i),zeta_coreA);
plot(ur_CoreA(i,:)/Umax_r(i),-zeta_coreA);
title(sprintf('Flow_profiles_of_a_round_channel_with_a_radius_of_
    %g_mm,\n_Umax_of_%g_mm/s_and_film_thickness_of_%g_mm',R,Umax_r
    (i),ho_r(i)),'fontsize',22);
ylabel('zeta_(r/R)','fontsize',22);
xlabel('U/Umax','fontsize',22);
    %axis([-1.1 1.1 -1.1 1.1]);
    pbaspect([2 2 1]);
set(gca, 'FontSize',20)

% Core B
plot(ur_CoreB(i,1:find(zeta_CoreB(i,:),1,'last'))/Umax_r(i),
    zeta_CoreB(i,1:find(zeta_CoreB(i,:),1,'last')),'g')
plot(ur_CoreB(i,1:find(zeta_CoreB(i,:),1,'last'))/Umax_r(i),-
    zeta_CoreB(i,1:find(zeta_CoreB(i,:),1,'last')),'g')
% film A
plot(ur_FilmA(i,1:find(zeta_FilmA(i,:),1,'last'))/Umax_r(i),
    zeta_FilmA(i,1:find(zeta_FilmA(i,:),1,'last')),'r')
plot(ur_FilmA(i,1:find(zeta_FilmA(i,:),1,'last'))/Umax_r(i),-
    zeta_FilmA(i,1:find(zeta_FilmA(i,:),1,'last')),'r')

print('-depsc','-r300','-loose',sprintf('figs/%s_flow_profile.
    eps',char(Ca_label_r(i))));
print('-dpdf','-r300','-loose',sprintf('figs/%s_flow_profile.
    pdf',char(Ca_label_r(i))));
    % saveas(gcf,sprintf('~/Research/bi-slug/Matlab/Final/figs/%
    s_flow_profile.eps',char(Ca_label(i))),'eps')
hold off
end % Round Channels

```

```
%
%%%%%%%%%%%%%%%%%%%%%%%%%%%%%%%%%%%%%%%%%%%%%%%%%%%%%%%%%%%%%%%%%%%%%%%%%
```

### Square Channels

Going to use the x value from the wall as the reference point for each calculation. Plots of profile on x and the normalized film velocity will be plotted.

```
Ca=[2E-3 4E-3]; % Data from experiments
Ca_label=cellstr(['Square_Prewet_low_'; 'Square_Prewet_high']);
%labels for the data
```

```
Umax=Ca*sigma_A/mu_A*1000 ; % mm/s
ho=R.*.643*(3.*Ca).^(2/3);
H=ho./R; % non dimensionalized film thickness H=ho/R
```

```
%outer loop, using k for an k,i,j arrays
for k=1:length(ho)
```

### Parameters

Using the same initial parameters as the round channels

### Flow in a square channel with a thin film

Two regions for both the Couette and Poiseuille flow There are two different functions for the distance to the film.

```
Rc=.1;
```

```
xf(k)=R-ho(k)-Rc; % the length from the
center to the transition point on the wall of the channel in
the x-dir
```

```
zeta_o_trans(k)=xf(k)/R ;% transition point from flat to curved
```

```
for i=1:length(0:(zeta_o_trans)/2:zeta_o_trans);
a=0:(zeta_o_trans(k))/2:zeta_o_trans(k);
zeta_s_flat(k,i)=a(i) ; % the range for the flat region on the
wall
end
clear a
```

---

```

Ho(k)=ho(k)/R;                                     % non-dimensional film
            thickness in the flat region, ho/R
% Flat region
for i=1:length(zeta_s_flat)

sigma_s_o_flat(k,i)=sqrt(zeta_s_flat(k,i).^2+1);
            % The length from the center to the
            wall

sigma_s_film_flat(k,i)=sigma_s_o_flat(k,i).*(1-Ho(k)) ;
            % Using similar triangles to find
            sigma_s_film_flat
end

% Curved region
C=Rc/R;

for i=1:length([zeta_o_trans(k),(1+zeta_o_trans(k))/2,1])
            % zeta_s_corner_wall
            a=[zeta_o_trans(k),(1+zeta_o_trans(k))/2,1];
zeta_s_corner_wall(k,i)=a(i);                    % range to of zeta on the
            wall

Hc(k,i)=sqrt((zeta_s_corner_wall(k,i)-zeta_o_trans(k)).^2+(C+Ho(k)
            )).^2)-C;                            % Hc based on zeta

Hc_prime(k,i)=Hc(k,i).*(C+Ho(k))./(C+Hc(k,i));    % Hc_prime
            based on zeta

zeta_s_corner_prime(k,i)=real(zeta_s_corner_wall(k,i)-sqrt(Hc(k,i)
            ).^2-Hc_prime(k,i).^2)); % This is for calcs of sigma film
            and sigma_s_o,

sigma_s_film_corner(k,i)=real(sqrt((1-Hc_prime(k,i)).^2+
            zeta_s_corner_prime(k,i).^2));

sigma_s_o_corner(k,i)=sigma_s_film_corner(k,i)./(1-Hc_prime(k,i))
            ;

zeta_s_corner_wall_acted(k,i)=sqrt(sigma_s_o_corner(k,i)^2-1);
            % This is the actual wall position that
            sigma_o is calced on

```

Velocity at the film, UAB for calcs

Flat

---

```

UAB_s_flat(k,i)=Umax(k)./(1-1/2.*muA/muB.*1./log(
    sigma_s_film_flat(k,i)./sigma_s_o_flat(k,i)));

% Corner
UAB_s_corner(k,i)=Umax(k)./(1-1/2.*muA/muB.*1./log(
    sigma_s_film_corner(k,i)./sigma_s_o_corner(k,i)));

end

%%%%%%%%%%%%%%%%%%%%%%%%%%%%%%%%%%%%%%%%%%%%%%%%%%%%%%%%%%%%%%%%%%%%%%%%%%%%%% Graphing Beginning
%%%%%%%%%%%%%%%%%%%%%%%%%%%%%%%%%%%%%%%%%%%%%%%%%%%%%%%%%%%%%%%%%%%%%%%%%%%%%%

Velocity at the film, UAB for graphing

Flat

for i=1:length([0:n:zeta_o_trans(k)])
    a=[0:n:zeta_o_trans(k)];
    zeta_s_flat_g(k,i)=a(i);
end
clear a

for i=1:length(zeta_s_flat_g(k,:))
    zeta_s_flat_so_g(k,i)=zeta_s_flat_g(k,i)/(1-Ho(k));
    sigma_s_film_flat_g(k,i)=sqrt(zeta_s_flat_g(k,i).^2+(1-Ho(k))^2);
    % The length from the center to the film
    sigma_s_o_flat_g(k,i)=sqrt(zeta_s_flat_so_g(k,i).^2+1);
    % The length from the center to the
    wall

UAB_s_flat_g(k,i)=Umax(k)./(1-1/2.*muA/muB.*1./log(
    sigma_s_film_flat_g(k,i)./sigma_s_o_flat_g(k,i)));

end

% Corner
for i=1:length([zeta_o_trans(k):n:1]) % range to of
    zeta on the wall for plotting
    a=[zeta_o_trans(k):n:1];
    zeta_s_corner_wall_g(k,i)=a(i);
end
clear a

```

```

for i=1:length(zeta_s_corner_wall_g(k,:))
Hc_g(k,i)=sqrt((zeta_s_corner_wall_g(k,i)-zeta_o_trans(k)).^2+(C+
    Ho(k)).^2)-C;           % Hc based on zeta
Hc_prime_g(k,i)=Hc_g(k,i).*(C+Ho(k))./(C+Hc_g(k,i));
                                % Hc_prime based on zeta
zeta_s_corner_prime_g(k,i)=real(zeta_s_corner_wall_g(k,i)-sqrt(
    Hc_g(k,i).^2-Hc_prime_g(k,i).^2)); % This is for calcs of
    sigma_film and sigma_s_o,
sigma_s_film_corner_g(k,i)=real(sqrt((1-Hc_prime_g(k,i)).^2+
    zeta_s_corner_prime_g(k,i).^2));
sigma_s_o_corner_g(k,i)=sigma_s_film_corner_g(k,i)./(1-Hc_prime_g
    (k,i));

UAB_s_corner_g(k,i)=Umax(k)./(1-1/2.*muA/muB.*1./log(
    sigma_s_film_corner_g(k,i)./sigma_s_o_corner_g(k,i)));

```

**end**

```

%%%%%%%%%%%%%%%%%%%%%%%%%%%%%%%%%%%%%%%%%%%%%%%%%%%%%%%%%%%%%%%%%%%%%%%%%%%%%% Graphing End
%%%%%%%%%%%%%%%%%%%%%%%%%%%%%%%%%%%%%%%%%%%%%%%%%%%%%%%%%%%%%%%%%%%%%%%%%%%%%%

```

### Poiseuille in Core B

Flat

```

for i=1:length(zeta_s_flat(k,:))

for j=1:length([0:n:1-Ho(k)]);
    a=[0:n:1-Ho(k)];
    psi_CoreB_flat(k,i,j)=a(j);

sigma_s_CoreB_flat(k,i,j)=psi_CoreB_flat(k,i,j).*sigma_s_o_flat(k
    ,i);
us_CoreB_flat(k,i,j)=(Umax(k)-UAB_s_flat(k,i)).*(1-
    sigma_s_CoreB_flat(k,i,j).^2./sigma_s_film_flat(k,i).^2)+
    UAB_s_flat(k,i);

```

**end**

**end**

**clear** a

% Corner

```

for i=1:length(zeta_s_corner_wall(k,:))
for j=1:length([0:n:1-Hc_prime(k,i)]);

    a=[0:n:1-Hc_prime(k,i)];
    psi_CoreB_corner(k,i,j)=a(j);

    sigma_s_CoreB_corner(k,i,j)=psi_CoreB_corner(k,i,j).*
        sigma_s_o_corner(k,i);
    us_CoreB_corner(k,i,j)=(Umax(k)-UAB_s_corner(k,i)).*(1-
        sigma_s_CoreB_corner(k,i,j).^2./sigma_s_film_corner(k,i).^2)+
        UAB_s_corner(k,i);

    end
l_CoreB_corner(k,i)=find(psi_CoreB_corner(k,i,:),1,'last');

end
clear a

```

### *Couette*

*% Flat*

*% Boundary for the film*

```

for i=1:length(zeta_s_flat(k,:))

    for j=1:length([1-Ho(k):n:1]);
        a=[1-Ho(k):n:1];
        psi_filmA_flat(k,i,j)=a(j);

        sigma_s_filmA_flat(k,i,j)=psi_filmA_flat(k,i,j).*
            sigma_s_o_flat(k,i);
        us_filmA_flat(k,i,j)=UAB_s_flat(k,i)*log(sigma_s_filmA_flat(k,i,j)
            )/sigma_s_o_flat(k,i))./log(sigma_s_film_flat(k,i)/
            sigma_s_o_flat(k,i));

    end
end
clear a

```

*% Corner*

---

```

for i=1:length(zeta_s_corner_wall(k,:));
for j=1:length([1-Hc_prime(k,i):n:1]);
    a=[1-Hc_prime(k,i):n:1];
    psi_filmA_corner(k,i,j)=a(j);

    sigma_s_filmA_corner(k,i,j)=psi_filmA_corner(k,i,j).*
        sigma_s_o_corner(k,i);
    us_filmA_corner(k,i,j)=UAB_s_corner(k,i)*log(
        sigma_s_filmA_corner(k,i,j)/sigma_s_o_corner(k,i))./log(
        sigma_s_film_corner(k,i)/sigma_s_o_corner(k,i));
end

l_filmA_corner(k,i)=find(psi_filmA_corner(k,i,:),1,'last');
end

clear a

end % end of the calculation loop

                                Core A, Poiseuille

for k=1:length(ho)
    for i=1:length(zeta_s_flat(k,:))
zeta_s_CoreA(k,i)=zeta_s_flat(k,i);    % non-dimensionlized x for
    Core A

    end
    for i=1:length(zeta_s_corner_wall(k,:))-1
zeta_s_CoreA(k,i+length(zeta_s_flat(k,:)))=zeta_s_corner_wall
        (k,i+1)
    end

end
sigma_s_o_CoreA=sqrt(1+zeta_s_CoreA.^2);    % the length from the
    center to the channel to the wall
for i=1:length(zeta_s_CoreA);

psi_s_CoreA=[0:n:1];

for j=1:length(psi_s_CoreA);

sigma_s_CoreA(k,i,j)=psi_s_CoreA(j).*sigma_s_o_CoreA(i);

```

---

```

us_CoreA(k,i,j)=Umax(k)*(1-sigma_s_CoreA(k,i,j).^2/
    sigma_s_o_CoreA(i).^2);

zeta_s_star_CoreA(k,i,j)=psi_s_CoreA(j)*zeta_s_CoreA(i);

end

end

% us_filmA_corner=UAB_s_corner*log(sigma_s_corner/
    sigma_s_o_corner)./log(sigma_s_film_corner/sigma_s_o_corner)

%%%%%%%%%%%%%%%%%%%%%%%%%%%%%%%%%%%%%%%%%%%%%%%%%%%%%%%%%%%%%%%%%%%%%%%%%%%%%% Beginning Graph for
    Square %%%%%%%%%%%%%%%%%%%%%%%%%%%%%%%%%%%%%%%%%%%%%%%%%%%%%%%%%%%%%%%%%%%%%%%%%%%%%%%

                                Plots in Square Channels

for k=1:length(ho)

                                Loop not needed for Core A

square w/o film

figure
hold on
% Core A

    for    i=1:length(zeta_s_CoreA(k,:));

plot(squeeze(us_CoreA(k,i,:))/Umax(k),squeeze(sigma_s_CoreA(k,i
    ,:)));
plot(squeeze(us_CoreA(k,i,:))/Umax(k),-squeeze(sigma_s_CoreA(k,i
    ,:)));
s{i}=sprintf('zeta=%g',zeta_s_CoreA(k,i));
    end

hold off

title(sprintf('Flow profiles of a square channel with a hydraulic
    diameter of %g mm \n and a Umax of %g mm/s at various
    locations along the channel',R,Umax(k)))
ylabel('sigma', 'fontsize',22);
xlabel('U/Umax', 'fontsize',22);
legend(s);
legend('boxoff','Best');
pbaspect([3 3 1]);

```

```

print ('-depsc', '-r300', '-loose', sprintf('figs/%s_flow_profile.eps',
    char(Ca_label(k))));
print ('-dpdf', '-r300', '-loose', sprintf('figs/%s_flow_profile.pdf',
    char(Ca_label(k))));
end

```

*Plots of flow in square channels with a thin film*

```

%%%% I need to add labels

```

```

    for k=1:length(ho); %starting here to minimize the time needed
        for testing individual loops
    % UAB, flow at the film
    figure
    hold on
    plot(sigma_s_o_flat_g(k,1:find(zeta_s_flat_g(k,:),1,'last')),
        UAB_s_flat_g(k,1:find(zeta_s_flat_g(k,:),1,'last'))/Umax(k))
    plot(sigma_s_o_corner_g(k,1:find(zeta_s_corner_wall_g(k,:),1,'
        last')),UAB_s_corner_g(k,1:find(zeta_s_corner_wall_g(k,:),1,'
        last'))/Umax(k))
    title(sprintf('The velocity at the film with a \n film thickness of
        %g mm and a Umax of %g',ho,Umax(k)))
    xlabel('sigma_o','fontsize',22)
    ylabel('Uab/Umax','fontsize',22)
    hold off
    print ('-depsc', '-r300', '-loose', sprintf('figs/%s_Uab.eps',char(
        Ca_label(k))));
    print ('-dpdf', '-r300', '-loose', sprintf('figs/%s_Uab.pdf',char(
        Ca_label(k))));

    figure
    hold on

    % flat

    for i=1:length(zeta_s_flat(k,:));
        % Core B Poiseuille
    plot(squeeze(us_CoreB_flat(k,i,1:find(psi_CoreB_flat(k,i,:),1,'
        last'))/Umax(k)),squeeze(sigma_s_CoreB_flat(k,i,1:find(
        psi_CoreB_flat(k,i,:),1,'last'))),'g');
    plot(squeeze(us_CoreB_flat(k,i,1:find(psi_CoreB_flat(k,i,:),1,'
        last'))/Umax(k)),-squeeze(sigma_s_CoreB_flat(k,i,1:find(
        psi_CoreB_flat(k,i,:),1,'last'))),'g');

    % Film A Couette flow

```

```

plot(squeeze(us_filmA_flat(k,i,1:find(psi_filmA_flat(k,i,:),1,'
    last')))/Umax(k),squeeze(sigma_s_filmA_flat(k,i,1:find(
    psi_filmA_flat(k,i,:),1,'last'))),'r');
plot(squeeze(us_filmA_flat(k,i,1:find(psi_filmA_flat(k,i,:),1,'
    last')))/Umax(k),-squeeze(sigma_s_filmA_flat(k,i,1:find(
    psi_filmA_flat(k,i,:),1,'last'))),'r');

s{i}=sprintf('zeta=%g',zeta_s_flat(k,i));
end

% curved

for i=1:length(zeta_s_corner_wall(k,:));

    % Core B Poiseuille
plot(squeeze(us_CoreB_corner(k,i,1:l_CoreB_corner(k,i))/Umax(k)),
    squeeze(sigma_s_CoreB_corner(k,i,1:l_CoreB_corner(k,i))),'b');
plot(squeeze(us_CoreB_corner(k,i,1:l_CoreB_corner(k,i))/Umax(k))
    ,-squeeze(sigma_s_CoreB_corner(k,i,1:l_CoreB_corner(k,i))),'b
    ');

    % Film A Couette flow
plot(squeeze(us_filmA_corner(k,i,1:l_filmA_corner(k,i))/Umax(k)),
    squeeze(sigma_s_filmA_corner(k,i,1:l_filmA_corner(k,i))),'r');
plot(squeeze(us_filmA_corner(k,i,1:l_filmA_corner(k,i))/Umax(k))
    ,-squeeze(sigma_s_filmA_corner(k,i,1:l_filmA_corner(k,i))),'r
    ');
% s{i}=sprintf('zeta=%g',zeta_s_flat(i)); %need to work on this
title(sprintf('Flow_profiles_of_a_square_channel_with_a_hydraulic
    diameter_of_%g_mm,a_film_thickness_of_%g_mm\n_and_a_Umax_of
    %g_mm/s_at_various_locations_along_the_channel',R,ho(k),Umax(
    k)))
end

% title(sprintf('Flow profiles of a square channel with a
    hydraulic diameter of %g mm, a film thickness of %g mm \n and
    a Umax of %g mm/s at various locations along the channel',R,ho
    ,Umax))
ylabel('sigma','fontsize',22);
xlabel('U/Umax','fontsize',22);
legend(s); % i need to work on the the legend
legend('boxoff','Best');
pbaspect([3 3 1]);
hold off

```



```

last ')), -psi_s_flat_profile(k, 1:find(zeta_s_flat_profile(k
, :) , 1, 'last ')), 'g')

plot( psi_s_flat_profile(k, 1:find(zeta_s_flat_profile(k, :) , 1, '
last ')), zeta_s_flat_profile(k, 1:find(zeta_s_flat_profile(k
, :) , 1, 'last ')), 'g')
plot(-psi_s_flat_profile(k, 1:find(zeta_s_flat_profile(k, :) , 1, '
last ')), -zeta_s_flat_profile(k, 1:find(zeta_s_flat_profile(k
, :) , 1, 'last ')), 'g')
    plot( psi_s_flat_profile(k, 1:find(zeta_s_flat_profile(k, :)
, 1, 'last ')), -zeta_s_flat_profile(k, 1:find(
zeta_s_flat_profile(k, :) , 1, 'last ')), 'g')
plot(-psi_s_flat_profile(k, 1:find(zeta_s_flat_profile(k, :) , 1, '
last ')), zeta_s_flat_profile(k, 1:find(zeta_s_flat_profile(k, :)
, 1, 'last ')), 'g')

% corner
plot(zeta_s_corner_profile(k, 1:find( psi_s_corner_profile(k, :) , 1,
'last ')), psi_s_corner_profile(k, 1:find( psi_s_corner_profile(k
, :) , 1, 'last ')), 'g')
plot(-zeta_s_corner_profile(k, 1:find( psi_s_corner_profile(k, :)
, 1, 'last ')), -psi_s_corner_profile(k, 1:find(
psi_s_corner_profile(k, :) , 1, 'last ')), 'g')
    plot(-zeta_s_corner_profile(k, 1:find( psi_s_corner_profile(k, :)
, 1, 'last ')), psi_s_corner_profile(k, 1:find(
psi_s_corner_profile(k, :) , 1, 'last ')), 'g')
plot(zeta_s_corner_profile(k, 1:find( psi_s_corner_profile(k, :) , 1,
'last ')), -psi_s_corner_profile(k, 1:find( psi_s_corner_profile(
k, :) , 1, 'last ')), 'g')

plot( psi_s_corner_profile(k, 1:find( psi_s_corner_profile(k, :) , 1, '
last ')), zeta_s_corner_profile(k, 1:find( psi_s_corner_profile(k
, :) , 1, 'last ')), 'g')
plot(-psi_s_corner_profile(k, 1:find( psi_s_corner_profile(k, :) , 1,
'last ')), -zeta_s_corner_profile(k, 1:find( psi_s_corner_profile
(k, :) , 1, 'last ')), 'g')
    plot( psi_s_corner_profile(k, 1:find( psi_s_corner_profile(k, :) , 1,
'last ')), -zeta_s_corner_profile(k, 1:find(
psi_s_corner_profile(k, :) , 1, 'last ')), 'g')
plot(-psi_s_corner_profile(k, 1:find( psi_s_corner_profile(k, :) , 1,
'last ')), zeta_s_corner_profile(k, 1:find( psi_s_corner_profile(
k, :) , 1, 'last ')), 'g')

```

```

% Lines of sigma_o
% flat

for i=1:length(zeta_s_flat(k,:));
    psi_profile=[0:n:1];
    for j=1:length(psi_profile)
        zeta_s_o_flat_profile(k,i,j)=zeta_s_flat(k,i)*psi_profile(j)./
            sigma_s_o_corner(k,i);
    end
    plot(squeeze(zeta_s_o_flat_profile(k,i,:)),psi_profile,'r');
    %text(max(zeta_s_o_flat_profile(k,i,:)),1,['\ zeta =',num2str(
        zeta_s_flat(k,i))]);
    text(max(zeta_s_o_flat_profile(k,i,:)),1.05,num2str(i))
    leg{i}=sprintf('%g=%g',i,max(zeta_s_o_flat_profile(k,i,:)))
end

% corner

for i=1:length(zeta_s_corner_wall(k,:));
    psi_profile=[0:n:1];
    for j=1:length(psi_profile)
        zeta_s_o_corner_profile(k,i,j)=psi_profile(j).*zeta_s_corner_wall
            (k,i);
    end
    plot(squeeze(zeta_s_o_corner_profile(k,i,:)),psi_profile,'r'
        );
    %text(max(zeta_s_o_corner_profile(k,i,:)),1,['\ zeta =',num2str(
        zeta_s_corner_wall_acted(k,i))]);
    text(max(zeta_s_o_corner_profile(k,i,:)),1.05,num2str(length(
        zeta_s_flat(k,:))+i));
    leg{length(zeta_s_flat(k,:))+i}=sprintf('%g=%g',length(
        zeta_s_flat(k,:))+i,max(zeta_s_o_corner_profile(k,i,:)))
end

% boundary of box
xwall=-1:n:1;
ywall=-1:n:1;
plot(-1,ywall,'b',1,ywall,'b',xwall,1,'b',xwall,-1,'b')

title(sprintf('Flow profiles of a square channel with a
    hydraulic diameter of %g mm, a film thickness of %g mm\n and

```

```

        Ca_Umax_of_%g_mm/s_at_various_locations_along_the_channel',R,
        ho(k),Umax(k))
T=legend(leg,'Location','SouthWest')
set(get(T,'title'),'String','Wall-Intercept')

pbaspect([3 3 1]);
hold off
print('-depsc','-r300','-loose',sprintf('figs/%
s_flow_profile_lines.eps',char(Ca_label(k))));
print('-dpdf','-r300','-loose',sprintf('figs/%
s_flow_profile_lines.pdf',char(Ca_label(k))));

end

```

Trying to find a relationship for  $H_c$

```

%close all
% for k=1:length(Ho)
%
% %figure
% % plotyy(sigma_s_o_corner_g(k,1:find(zeta_s_corner_wall_g(k,:))
% ,1,'last'),UAB_s_corner_g(k,1:find(zeta_s_corner_wall_g(k,:))
% ,1,'last'),sigma_s_o_corner_g(k,1:find(zeta_s_corner_wall_g(k,
% :)),1,'last'),(Hc_g(k,1:find(zeta_s_corner_wall_g(k,:)),1,'
% last')+Hc_prime_g(k,1:find(zeta_s_corner_wall_g(k,:)),1,'last
% ')).^(1/3)/2)
% %plot(sigma_s_o_corner_g(k,1:find(zeta_s_corner_wall_g(k,:))
% ,1,'last'),Hc_g(k,1:find(zeta_s_corner_wall_g(k,:)),1,'last')
% , 'g')
%
% % figure
% % [AX,H1,H2]= plotyy(sigma_s_o_corner_g(k,1:find(
% zeta_s_corner_wall_g(k,:)),1,'last'),UAB_s_corner_g(k,1:find(
% zeta_s_corner_wall_g(k,:)),1,'last'),sigma_s_o_corner_g(k,1:
% find(zeta_s_corner_wall_g(k,:)),1,'last'),(Hc_g(k,1:find(
% zeta_s_corner_wall_g(k,:)),1,'last')).^(1/3))
% % set(AX(1),'YLim',[.1 .8])
% % set(AX(2),'YLim',[.1 .8])
% % title(sprintf('Flow profiles of a square channel with a
% hydraulic diameter of %g mm, a film thickness of %g mm \n and
% a Umax of %g mm/s at various locations along the channel',R,ho
% (k),Umax))
%
% % figure
% % hold on
% % plot(sigma_s_o_corner_g(k,1:find(zeta_s_corner_wall_g(k,:)),1,
% 'last'),UAB_s_corner_g(k,1:find(zeta_s_corner_wall_g(k,:)),1,
% 'last')/Umax(k),'b')

```

```

% plot(sigma_s_o_corner_g(k,1:find(zeta_s_corner_wall_g(k,:),1,'
    last')), (Hc_g(k,1:find(zeta_s_corner_wall_g(k,:),1,'last')),
    'g')
%
% title(sprintf('Flow profiles of a square channel with a
    hydraulic diameter of %g mm, a film thickness of %g mm \n and
    a Umax of %g mm/s at various locations along the channel',R,ho
    (k),Umax(k)))
% ylim('auto')
% hold off
% print('-depsc','-r300','-loose',sprintf('~\Research/bi-slug/
    Matlab/Final/figs/%s-Hc.eps',char(Ca_label(k))));
% end

```

## D.2 derivation

```

clear, clc, close all
set(0,'DefaultFigureWindowStyle','docked')
set(0,'DefaultFigurePaperOrient','landscape')

```

*Integration of the different sections of the square channel for use in a model*

```

% Each part needs to be integrated, there may not be a closed
    solution
% which would require numerical integration.

```

*Flow in Core A in the square channel*

*Core A Parameters*

```

syms u_a U_max s_a so_a mu_a zeta_a z l_a
% u_a is the velocity in the channel
% U_max is the center line velocity
% s_a is the length from the center point to any location in the
    channel
% so_a is the length from the center point to the wall
% mu_a is the viscosity of fluid A
% zeta_a is the non-dimensional distance on the wall, x/R
% z is the direction of the slug length
% l_a is the length of the slug

```

*Equations for Core A*

```

u_a=U_max*(1-s_a^2/so_a^2); % the function for the velocity in
    Core A in the square channel

```

```

u_a_prime=diff(u_a,s_a); % du/ds

```

```

tau_w_a=mu_a*subs(u_a_prime,s_a,so_a); % the
    shear stress at the wall, mu_a*du/ds |s=so

```

```

% drag
sigmao_a_zeta=sqrt(1+zeta_a^2); %
    so_a non dimensionalized with R, zeta=x/R as a function of
    zeta

F_drag_a_dz_dzeta=int(subs(tau_w_a,so_a,sigmao_a_zeta),z,0,l_a);
    % Drag force in Core a in the square channel.
    evaluate for dz from 0-L for z

F_drag_a_dzeta=int(F_drag_a_dz_dzeta,zeta_a,0,1);
    % Drag force in Core a
    evaluated for dzeta from 0-1
F_drag_a=8*F_drag_a_dzeta; %
    solution simplifies the solution by putting the negative in
    the log term

fprintf('The solution, %s has the negative factor in the log term
, this matches the solution done by hand', 'F_drag_a')

```

#### Core B and Film A

Core B and Film A are dependent on each other

#### Core B and Film A Parameters

```

syms u_b_f mu_b U_AB u_film so sf sigmao sigmaf sigma R l_b Ho
zeta
% u_b velocity of the core b in the flat region zeta_trans
% mu_b viscosity of the fluid in core b
% U_AB velocity at the film in the flat region
% u_film velocity of the film a in the flat region
% so is the distance from the center to the wall
% sf is the distance from the center to the film
% sigmao is the nondimensional form of so , so/R
% sigmaf is the nondimensional form of sf , sf/R
% R is the Length of the half the wall
% l_b is the length of the slug in COre B, the film is located in
    this region
% Ho nondimensionalized film thickness ho, ho/R
% zeta is the nondimensionalized distance on the wall, x/R
% zeta_trans is the nondimensionalized distance to the transition
    between the flat and curved region

```

#### Equations for the velocities

---

```

U_AB=U_max/(1+1/2*mu_a/mu_b*1/log(sigmao/sigmaf)); % velocity at
    the film in the flat region, using the non-dimensional form

u_film=U_AB*log(sigmao/sigma)/log(sigmao/sigmaf); % velocity
    of the film as a function of sigma_f

u_b=(U_max-U_AB)*(1-sigma^2/sigmaf^2)+U_AB;

fprintf('solution_for_%s_is_the_same_as_my_hand_derivation,_have_
    to_use_matlab_to_group_and_collect\n\n','u_b')
fprintf('solution_for_%s_is_the_same_as_my_hand_derivation\n\n','
    u_film')

% find shear stress

u_b_prime=diff(u_b,sigma)/R ; % du/dsigma dsigma
    =ds/R dsigma*R=ds
u_film_prime=diff(u_film,sigma)/R ; % du/dsigma dsigma=ds
    /R

tau_b=collect(mu_b*subs(u_b_prime,sigma,sigmaf),U_max);
    % shear stress at the film, using collect on U_max
    to match my solutions
tau_film=collect(mu_a*subs(u_film_prime,sigma,sigmao),U_max) ;
    % shear stress at the wall, using collect on U_max
    to match my solutions

% integrating to find shear stress

% fdrag=8*int*int tau_a dz dzeta
% dz is the differential length of the slug
% dzeta=dx/R

Fdrag_b_dz_dzeta=int(tau_b,z,0,l_b);
Fdrag_film_dz_dzeta=int(tau_film,z,0,l_b) ; %First integration
    of the drag in the flat regions, int dz | 0-l_b

sigmao_f=sqrt(zeta^2+1); % distance from the
    center to the wall for the flat region

sigmaf_f1=sigmao_f*(1-Ho); %
    Trial Fix
sigmaf_f=sqrt(zeta^2+(1-Ho)^2) ; % distance
    from the center to the film for the flat region

FINDING U_AB_F %%%%
```





```

C='Rc'/R; % C=Rc/R
Hc=sqrt((zeta-'zeta_trans').^2+(C+'Ho')^2)-C;
zeta_x=zeta-Hc*(zeta-'zeta_trans')/(C+Hc); %
    distance to the film normal to the film at the wall
Hc_prime=(C+'Ho')/(C+Hc)*Hc; %
    thickness normal to the wall through the film

sigmaf_c=sqrt(zeta_x^2+(1-Hc_prime)^2); % Distance
    to film based on zeta and ho and Rc
U_AB_c=subs(subs(U_AB,sigmao,sigmao_c),sigmaf,sigmaf_c);

%%%%%%%%%%%%%%%%%%%%%%%%%%%%%%%%%%%%%%%%%%%%%%%%%%%%%%%%%%%%%%%%%%%%%%%%
%%%%%%%%%%%%%%%%%%%%%%%%%%%%%%%%%%%%%%%%%%%%%%%%%%%%%%%%%%%%%%%%%%%%%%%%
                                Corner Core B

% For integrating across the film the perpedicular to the surface
% is used

sigmao_c=sqrt(zeta.^2+1);
T_b_c=-2*U_max*l_b;
for i=1:length(Ho_o);
    Ho=Ho_o(i);
    C=Rc./R_chan; % C=Rc/R
    Hc=sqrt((zeta-zeta_trans(i)).^2+(C+Ho).^2)-C; %%%
    ADDED -C
    Hc_prime=(C+Ho)./(C+Hc).*Hc; %
    thickness normal to the wall through the film
    %zeta_x=zeta-Hc.*(zeta-zeta_trans(i))./(C+Hc); %
    distance to the film normal to the film at the wall
    zeta_x=zeta-sqrt(Hc^2-Hc_prime^2);

    sigmaf_c(i)=sigmao_c*(1-Hc_prime); % Distance to
    film based on zeta and ho and Rc
    %sigmaf_c(i)=sqrt(zeta_x.^2+(1-Hc_prime).^2); %
    Distance to film based on zeta and ho and Rc

Fdrag_b_c_dzeta(i)=subs(subs(subs(subs(Fdrag_b_dz_dzeta,sigmao,
    sigmao_c),sigmaf,sigmaf_c(i)),R,R_chan); % subbed in
    sigmao sigmaf and mu_a and mu_b

Fdrag_b_c_dzeta_string=char(vectorize(Fdrag_b_c_dzeta(i)));

Hc_prime_end=(C+Ho)./(C+(sqrt((1-zeta_trans(i)).^2+(C+Ho).^2)-C))
    .* (sqrt((1-zeta_trans(i)).^2+(C+Ho).^2)-C); %

```

```

    position of end of meniscus
zeta_end_c=1-Hc_prime_end;

%Fdrag_b_c_dzeta_int(i)=quad(Fdrag_b_c_dzeta_string , zeta_star_f ,
    zeta_end_c);
Fdrag_b_c_dzeta_int(i)=quad(Fdrag_b_c_dzeta_string , zeta_trans(i) ,
    zeta_end_c);
end
Fdrag_b_c=8*T_b_c*Fdrag_b_c_dzeta_int;

```

### Corner Film A

```

% Film will use the same definitions for sigma_f and sigma_o and
    mu_a and
% mu_b
T_film_c=-U_max*l_b;
for i=1:length(Ho_o);

    FIX sigma_f_c, current version uses sigma_x which is for the core

Fdrag_film_c_dzeta(i)=subs(subs(subs(subs(Fdrag_film_dz_dzeta ,
    sigma_o , sigma_o_c) , sigma_f , sigma_f_c(i))/T_film_c) ,R,R_chan); %
    subbed in sigma_o sigma_f and mu_a and mu_b
Fdrag_film_c_dzeta_string=char(vectorize(Fdrag_film_c_dzeta(i)));

zeta_trans_c(i)=zeta_trans(i);
Fdrag_film_c_dzeta_int(i)=quad(Fdrag_film_c_dzeta_string ,
    zeta_trans_c(i) ,1);
end

Fdrag_film_c=vpa(8*Fdrag_film_c_dzeta_int*subs(T_film_c ,R,R_chan)
    ,5);

```

### Round

```

clear ho=1 syms tau_w_round_core mu_a mu_b Ho_o U_max U_ab l_b R_chan

for i=1:length(ho)
    U_ab(i)=U_max./(1-mu_a./(2*mu_b)./log(1-Ho_o(i)));

    tau_f_round_core(i)=-2*mu_b*(U_max-U_ab(i))./(R_chan*(1-Ho_o(i)));
Fdrag_round_core(i)=collect(tau_f_round_core(i)*l_b*2*pi*(1-
    Ho_o(i))*R_chan ,U_max) ; %Tau_w*area of contact
    with the wall
tau_w_round_film(i)=-mu_a*U_ab(i)/R_chan/log(1/(1-Ho_o(i)));
tau_f_round_film(i)=-mu_a*U_ab(i)/(R_chan*(1-Ho_o(i)))/log
    (1/(1-Ho_o(i)));

```

```

Fdrag_round_film(i)=tau_w_round_film(i)*l_b*2*pi*R_chan ;
                                %Tau_w*area of contact with the
                                wall
end

```

### Plotting Drag and ho

```

% separate square with film
figure
hold on
plot(ho(3:length(ho)),Fdrag_b_f_int(3:length(ho))*2*8,ho(3:length(ho)),
      Fdrag_b_c_dzeta_int(3:length(ho))*2*8,ho(3:length(ho)),
      Fdrag_film_f_int(3:length(ho))*8,ho(3:length(ho)),
      Fdrag_film_c_dzeta_int(3:length(ho))*8);
plot(ho(1:2),Fdrag_b_f_int(1:2))*2*8,ho(1:2),Fdrag_b_c_dzeta_int(1:2))*2*8,ho(1:2),
      Fdrag_film_f_int(1:2))*8,ho(1:2),
      Fdrag_film_c_dzeta_int(1:2))*8);
hold off
% plot(ho,Fdrag_b_f_int*8*R_chan)
% plot(ho,Fdrag_b_c_dzeta_int*8*R_chan)
% plot(ho,Fdrag_film_f_int*8*R_chan)
% plot(ho,Fdrag_film_c_dzeta_int*8*R_chan)
% plot(ho,(Fdrag_b_c_dzeta_int+Fdrag_b_f_int)*8*R_chan)
% plot(ho,(Fdrag_film_c_dzeta_int+Fdrag_film_f_int)*8*R_chan)

title('F_d_r_a_g_a_s_a_function_a_s_h_o_in_a_square_channel');
ylabel('Fdrag, -#*Umax*l_b');
xlabel('ho');
legend('F_d_Core_flat','F_d_Core_corner','F_d_film_flat','F_d_film_corner');

% hold off

% total square with film

figure
hold on
plot(ho(3:length(ho)),(Fdrag_b_c_dzeta_int(3:length(ho))+
      Fdrag_b_f_int(3:length(ho)))*2*8,ho(3:length(ho)),(
      Fdrag_film_c_dzeta_int(3:length(ho))+Fdrag_film_f_int(3:length(ho)))*8,ho(3:length(ho)),((Fdrag_b_c_dzeta_int(3:length(ho))+
      Fdrag_b_f_int(3:length(ho)))*2*8+(Fdrag_film_c_dzeta_int(3:length(ho))+Fdrag_film_f_int(3:length(ho)))*8));
plot(ho(1),(Fdrag_b_c_dzeta_int(1)+Fdrag_b_f_int(1))*2*8,'o',ho(1),(Fdrag_film_c_dzeta_int(1)+Fdrag_film_f_int(1))*8,'o',ho(1),((Fdrag_b_c_dzeta_int(1)+Fdrag_b_f_int(1))*2*8+(Fdrag_film_c_dzeta_int(1)+Fdrag_film_f_int(1))*8),'o',')

```

```

    MarkerSize',10,'MarkerFaceColor','green','MarkerEdgeColor','k'
    );
plot(ho(2),(Fdrag_b_c_dzeta_int(2)+Fdrag_b_f_int(2))*2*8,'square'
    ,ho(2),(Fdrag_film_c_dzeta_int(2)+Fdrag_film_f_int(2))*8,'
    square',ho(2),((Fdrag_b_c_dzeta_int(2)+Fdrag_b_f_int(2))*2*8+(
    Fdrag_film_c_dzeta_int(2)+Fdrag_film_f_int(2))*8),'square','
    MarkerSize',10,'MarkerFaceColor','green','MarkerEdgeColor','k'
    );

hold off
title('Total_F_d_r_a_g_as_a_function_as_h_o_in_a_square_channel')
ylabel('F_d_r_a_g, -#*U_max*l_b')
xlabel('h_o')
legend('Total_F_d_Core','Total_F_d_Film','Total_F_d_r_a_g')
print('-depsec','-r300','-loose','figs/total_drag_square.eps');
print('-dpdf','-r300','-loose','figs/total_drag_square.pdf');

% Round with film
a=double(vpa(Fdrag_round_core)/-U_max/l_b);
b=double(Fdrag_round_film/-U_max/l_b);

% Separate
figure
hold on
plot(ho(3:length(ho)),a(3:length(ho)),ho(3:length(ho)),b(3:length
    (ho)),ho(3:length(ho)),a(3:length(ho))+b(3:length(ho)));
plot(ho(1:2),a(1:2),ho(1:2),b(1:2),ho(1:2),a(1:2)+b(1:2));
hold off
title('F_d_r_a_g_as_a_function_as_h_o_in_a_round_channel');
ylabel('Fdrag, -#*U_max*l_b');
xlabel('h_o');
legend('F_d_Core','F_d_film','Total_F_d');

print('-depsec','-r300','-loose','figs/total_drag_round.eps');
print('-dpdf','-r300','-loose','figs/total_drag_round.pdf');

```

#### Table Production

```

%table1=['ho','Round F_drag Coefficient']
table1=[ho',(a+b)']
csvwrite('Round_drag_coefficient_ho_drag.csv',table1);

%table2=['ho','Square F_drag Coefficient']
table2=[Ca_bound(1:2)',ho(1:2)',((Fdrag_b_c_dzeta_int(1:2)+
    Fdrag_b_f_int(1:2))*2*8+(Fdrag_film_c_dzeta_int(1:2)+
    Fdrag_film_f_int(1:2))*8)'];
csvwrite('square_drag_coefficient_ho_drag.csv',table2);

```

*Force Balance*

*Stretch Term*

```
clear mu_a
syms sigma_a sigma_ab C_B H_B sigma_b x_f H_A alpha R U_max l_a
l_b beta mu_a
```

```
F_stretch=2*pi*R*((1-H_A/R)*(sigma_b+sigma_ab-sigma_a)-x_f/R*(
sigma_b+sigma_ab)-sigma_b*H_B/R)+8*x_f*(sigma_ab+sigma_b);
```

*Pressure Term*

```
delP=2*(sigma_a-sigma_ab-sigma_b)/R;
A_men=pi*R^2;
```

```
F_press=delP*A_men;
```

*Sum Terms*

```
a=F_press; % Pressure Force
b=F_stretch; %Stretch Terms
c=alpha*U_max*l_b; %Total Drag for trailing slug and
film
d=beta*mu_a*U_max*l_a; % Drag for
in Core A
```

*%Without Stretch*

```
total_wostretch=c+d-a;
U_maxwostretch=solve(total_wostretch,U_max);
pretty(U_maxwostretch);
```

*%With stretch*

```
Total_stretch=b+c+d-a ; % term is equal to zero
at this point
U_max_stretch=solve(Total_stretch,U_max);
pretty(U_max_stretch);
```

*Data for plots, with and without stretch*

```
R=R_chan
```

```
sigma_A=47.7;
sigma_B=20.3;
sigma_AB=18.0;
```

```
mu_a=0.0178; % kg/(m s)
mu_A=mu_a;
```

```

alpha=[((Fdrag_b_c_dzeta_int(1:2)+Fdrag_b_f_int(1:2))*2*8+(
    Fdrag_film_c_dzeta_int(1:2)+Fdrag_film_f_int(1:2))*8)];
beta=-16*log(2^(1/2)-1);

L_A=[1:1:25];
%L=[.5,1.2]
L=1
% without
for i=1:2
Ca_max_nostretch(i,:)=2.*pi.*R./L_A.*(1-(sigma_B+sigma_AB)/
    sigma_A)/(alpha(i)./mu_A*L + beta);
end

%with
xf=R.chan-Rc-ho;
for i=1:2
    ha=ho(i)
    Ca_max_stretch(i,:)= 2.*pi.*R./L_A.*((1-(sigma_B+sigma_AB)/
        sigma_A)*(2-ha/R)+xf(i)/R*(1-4/pi)*((sigma_B+sigma_AB)/
        sigma_A))/(alpha(i)./mu_A*L + beta)
end

Ca_data_front=csvread('10_19_07_square.csv',1,4);
L_A_data=csvread('10_19_07_square.csv',1,1,[1,1,29,1]);
L_B_data=csvread('10_19_07_square.csv',1,2,[1,2,29,2]);

figure
hold on
plot(L_A,Ca_max_nostretch(1,:), 'o', 'MarkerEdgeColor', 'black');
plot(L_A,Ca_max_nostretch(2,:), '^', 'MarkerEdgeColor', 'green');
plot(L_A,Ca_max_stretch(1,:), 'square', 'MarkerEdgeColor', 'blue');
plot(L_A,Ca_max_stretch(2,:), 'v', 'MarkerEdgeColor', 'm');
plot(L_A_data,Ca_data_front, '+', 'MarkerEdgeColor', 'red');
hold off
h_legend=legend('Low_Ca_Prediction ,_no_stretch', 'High_Ca_
    Prediction ,_no_stretch', 'Low_Ca_Prediction ,_stretch', 'High_Ca_
    Prediction ,_stretch', 'Experimental_Data', 'Location', 'SouthWest
    ');
set(h_legend, 'FontSize', 8)
xlabel('L_A_(mm)')
ylabel('Ca_Number(U_{max})_\mu_A/_\sigma_A')
set(gca, 'XMinorTick', 'on', 'Yscale', 'log', 'Xscale', 'log');

```

```

xlim([.7,50]);
ylim([.0005,.05]);

print('-depsec','-r300','figs/square_data_compare_front.eps');
print('-dpdf','-r300','figs/square_data_compare_front.pdf');

Ca_data_rear=csvread('10_19_07_square.csv',1,6);

figure
hold on
plot(LA,Ca_max_nostretch(1,:), 'o', 'MarkerEdgeColor','black');
plot(LA,Ca_max_nostretch(2,:), '^', 'MarkerEdgeColor','green');
plot(LA,Ca_max_stretch(1,:), 'square', 'MarkerEdgeColor','blue');
plot(LA,Ca_max_stretch(2,:), 'v', 'MarkerEdgeColor','m');
plot(LA_data,Ca_data_rear, '+', 'MarkerEdgeColor','red');
hold off
h_legend=legend('Low_Ca_Prediction','no_stretch','High_Ca_Prediction','no_stretch','Low_Ca_Prediction','stretch','High_Ca_Prediction','stretch','Experimental_Data','Location','SouthWest');
set(h_legend,'FontSize',8)
xlabel('LA(mm)')
ylabel('Ca_Number(U_{max})_{\mu_A}/_{\sigma_A}')
set(gca,'XMinorTick','on','Yscale','log','Xscale','log');
xlim([.7,50]);
ylim([.0005,.05]);

print('-depsec','-r300','figs/square_data_compare_rear.eps');
print('-dpdf','-r300','figs/square_data_compare_rear.pdf');

```